© 2025. Published by The Company of Biologists | Development (2025) 152, dev204762. doi:10.1242/dev.204762

RESEARCH ARTICLE

Enhanced RNA quality control maintains long-term regenerative ability in planarians

Michael Zelko[1,*,§], Danyan Li[1,‡,§], Sudheesh Allikka Parambil[1], Axel Poulet[1], Andrew Verdesca[1], Kaspar Mazeika[1], Krishnakali Dasgupta[1] and Josien C. van Wolfswinkel[1,2,3,4,¶]

ABSTRACT

Planarians have proficient regenerative abilities that persist undiminished throughout adulthood, mediated by their stem cells (neoblasts). It is unclear how planarians accomplish this, as most animals show age-related declines in health and regeneration. Neoblasts express the conserved RNA regulatory PIWI protein SMEDWI-1, homologs of which are found in germ cells and long-lived cells in other systems. We previously found that loss of SMEDWI-1 from the neoblasts results in accumulation of non-coding and aberrant RNAs. Here, we report that, over time, SMEDWI-1-depleted animals develop defects in wound repair and regeneration, alterations in secreted proteins, and increased intracellular protein aggregation. Our data indicate that these defects result from misassembly of the signal recognition particle (SRP), a ribonucleoprotein (RNP) responsible for co-translational protein secretion that contains a non-coding RNA as a scaffold. In the absence of tight regulation of non-coding RNA, as provided by SMEDWI-1, gradual accumulation of RNAs leads to imbalances in essential cellular machinery such as the SRP, resulting in compromised proteostasis and progressive loss of organismal vigor.

KEY WORDS: Regeneration, RNA control, PIWI protein, Non-coding RNA, Proteostasis, Aging

INTRODUCTION

Wound repair and regeneration are crucial processes in organismal life. At the end of embryonic development, the main structures that make up the adult organism have been formed, but developmental processes continue to play an essential role in body maintenance. The cells and structures of an organism inevitably sustain damages over time, both from internal and external origins, resulting in diminished tissue health and increased organismal fragility. To maintain function and ultimately viability, lesions need to be repaired, cells need to be replaced and structures need to be rebuilt. Wound healing and regeneration thus are crucial to maintain organismal integrity and extend organismal life.

While injuries and damage accumulate over time, organismal regenerative abilities typically decrease with age, resulting in a progressive decline in organismal health, commonly known as aging. Remarkably, some animals, such as the planarian *Schmidtea mediterranea*, appear able to maintain organismal health indefinitely (Deere et al., 2024; Gambino et al., 2020; Mouton et al., 2011; Oviedo et al., 2008; Perrigue et al., 2015; Sahu et al., 2017). *S. mediterranea* has an undetermined lifespan, and does not show a decrease in regenerative ability or wound repair with age. This is in large part ascribed to the presence of a population of adult stem cells called neoblasts, which allow the animals to continuously replace any aged or damaged cells with new specimens (Reddien and Sanchez Alvarado, 2004). This implies that the neoblasts of *S. mediterranea* need to maintain their functional integrity for extended periods of time. In the asexual strain of *S. mediterranea*, which does not generate mature germ cells and thus always remains in its adult stage, the neoblast population has sustained the animals for millions of years, without detectable decline (Lázaro et al., 2011), suggesting that the degenerative processes that plague other cell types do not occur in the planarian neoblasts. Understanding how the neoblasts keep such processes at bay could provide new insights into the etiology of aging, as well as extend our understanding of the processes involved in cellular maintenance.

One of the few proteins that are consistently and specifically present in the adult stem cells of such long-lived and highly regenerative animals are PIWI proteins (Sturm et al., 2017; van Wolfswinkel, 2014). These RNA-binding proteins use a small non-coding RNA called a piRNA to guide them to specific nucleotide sequences and suppress these, by inducing mRNA degradation or chromatin-based silencing (Czech et al., 2018; Haase et al., 2024). Their best-known targets are transposon sequences, but many other targets have been proposed. Whether these proteins have a role in upholding the negligible senescence of long-lived animal systems and, if so, how that would be accomplished, remains unknown.

We recently studied the role of the stem cell-specific PIWI protein SMEDWI-1 in the functioning of planarian neoblasts. We found that in the absence of SMEDWI-1, transposons remain repressed, but the RNA health of the neoblasts is no longer upheld (Allikka Parambil et al., 2024). Without SMEDWI-1, various non-coding and dysfunctional RNAs accumulate in the neoblasts without significant changes to the transcription of these molecules, indicating that SMEDWI-1 functions in the post-transcriptional quality control of these RNA transcripts.

Here, we report that SMEDWI-1-depleted animals over time develop a macroscopic phenotype that compromises their long-term health: upon extended knockdown of SMEDWI-1, animals acquire inefficiencies in wound closure, show ineffective regeneration, and become fragile, reminiscent of the deterioration of wound repair

[1]Department of Molecular Cellular and Developmental Biology, Yale University, New Haven, CT 06511, USA. [2]Yale Stem Cell Center, Yale School of Medicine, New Haven, CT 06511, USA. [3]Yale Center for RNA Science and Medicine, Yale School of Medicine, New Haven, CT 06511, USA. [4]Yale Center for Aging Research (Y-AGE), Yale School of Medicine, New Haven, CT 06511, USA.
*Present address: Cell Molecular Biology Graduate Program, University of Chicago, Chicago, IL 60637, USA. ‡Present address: Department of Basic Medical Sciences, School of Medicine, Tsinghua University, Beijing, China.
§These authors contributed equally to this work

¶Author for correspondence (josien.van.wolfswinkel@yale.edu)

J.C.v.W., 0000-0003-4221-3218

Handling Editor: Mansi Srivastava
Received 2 March 2025; Accepted 4 September 2025

Development (2025) 152, dev204762. doi:10.1242/dev.204762

and regeneration that commonly occurs in aging systems. Our analysis of this phenomenon points towards defects in protein secretion as the underlying cause. The connection between RNA fidelity and protein secretion runs through the signal recognition particle (SRP), which is a ribonucleoprotein (RNP) complex whose stoichiometry and assembly is affected by the overall RNA defect in *smedwi-1(RNAi)* animals. Our data indicate that the misregulation of RNA integrity (such as by the loss of SMEDWI-1) induces widespread effects that extend to deregulation of proteostasis and can result in progressive organismal fragility. This study emphasizes the importance of non-coding RNA in cellular function, and the importance of RNA control mechanisms for maintaining long-term cellular and organismal health.

RESULTS

Depletion of SMEDWI-1 results in defective regeneration

SMEDWI-1 is a stem cell-specific PIWI protein that is commonly used as a stem cell marker in *S. mediterranea* (Palakodeti et al., 2008; Reddien et al., 2005). We recently reported that SMEDWI-1 enhances the resilience of the neoblast population (Allikka Parambil et al., 2024). However, we noticed an additional phenotype when knockdown of SMEDWI-1 was continued beyond the typical 3-week time span. Sexual animals that received more than 2 months of *smedwi-1* RNAi treatment demonstrated frequent epidermal blistering, wound closure defects, arrested regeneration and lysis of tissue fragments. To represent the spectrum of regeneration phenotypes of *smedwi-1(RNAi)* animals, we created a phenotype scale where 3-day blastemas with normal size and morphology were assigned a score of 0, while blastemas with signs of rupture were represented by a score of 1, and wounds that failed to close at all were given a score of 2 (Fig. 1A). After 2 months of *smedwi-1(RNAi)* treatment, nearly half of the animals failed to close their wounds after amputation, and after 3 months this increased to over 80% (Fig. 1B). Follow-up of such animals showed that tissue fragments with unclosed wounds did not complete regeneration and eventually died. Wound closure defects were primarily observed among fragments with a large wound

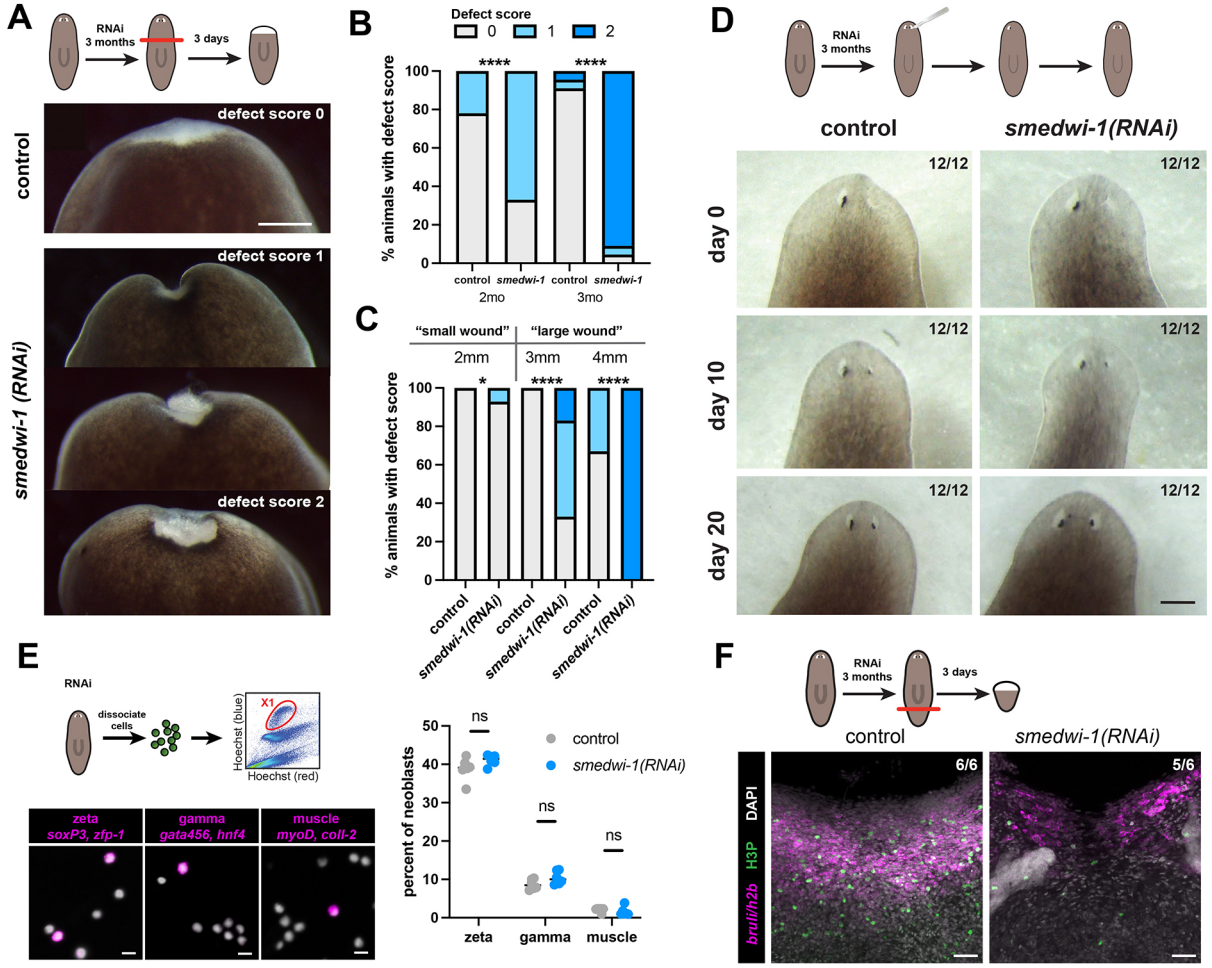

Fig. 1. Loss of SMEDWI-1 leads to impaired wound healing. (A) Live images showing the wound healing phenotypes at day 3 (d3) after amputation in long-term *smedwi-1(RNAi)* animals. Scale bar: 1 mm. (B) Quantification of observed wound-healing phenotypes at d3 post-amputation relative to the duration of the *smedwi-1(RNAi)* treatment (>50 animals per condition; Fisher's exact test, ****P<0.0001). (C) Quantification of observed wound-healing phenotypes at d3 post-amputation relative to the wound size in control and *smedwi-1(RNAi)* animals (>20 animals per condition; Fisher's exact test, *P<0.05, ****P<0.0001). (D) Live images showing the progression of eye regeneration in *smedwi-1(RNAi)* animals compared to controls. Scale bar: 1 mm. (E) Fluorescent *in situ* hybridization (FISH) on isolated neoblasts (X1) from *smedwi-1(RNAi)* animals and controls, showing several classes of lineage-specified neoblasts (left) and quantification (right). Scale bars: 10µm. Statistical analysis was carried out using a paired *t*-test; ns, not significant (6 biological replicates per RNAi, >100 cells analyzed per replicate). (F) Immunofluorescence of phosphorylated histone 3 (H3P) and FISH of *bruli* and *h2b* mark neoblasts at day 3 after amputation of large posterior fragments. *smedwi-1(RNAi)* fragments have reduced accumulation of neoblasts at the wound site. Scale bars: 50 µm.

Development (2025) 152, dev204762. doi:10.1242/dev.204762

diameter (Fig. 1C), and therefore were most apparent in large sexual animals. However, the regeneration defects were not due to effects on the germline, as *nanos(RNAi)* animals that lacked a germline (Wang et al., 2007) showed no defect in regeneration, whereas defects in *smedwi-1 nanos(double RNAi)* animals were comparable to those of size-matched *smedwi-1(RNAi)* animals (Fig. S1A). Further, phenotypes could be reproduced in asexual animals: the effect on transverse wounds was milder due to their smaller size (Fig. S1B), but parasagittal amputations confirmed a penetrant defect in *smedwi-1(RNAi)* asexual animals (Fig. S1C). The *smedwi-1(RNAi)* defect in wound closure and regeneration in asexual animals further presented as reduced ability of animal colonies to expand, as increased incidence of morphological defects, and as increased fragility in the face of microbial exposure (Fig. S2A-D). We therefore conclude that long-term depletion of SMEDWI-1 leads to defects in wound closure and blastema integrity, leading to organismal fragility.

SMEDWI-1 depletion does not impair the proliferation or specification of neoblasts

We previously found that homeostatic expression of stem cell genes was not significantly altered in *smedwi-1(RNAi)* animals (Allikka Parambil et al., 2024). We therefore expected that the wound regeneration defect would not originate from general defects in stem cell function, but rather from the response to wounding. We made several observations that support this notion.

First, we confirmed that no major changes in neoblast transcripts or in transposon expression were detected upon long-term suppression of *smedwi-1* (Fig. S1D,E). Second, we found that minor wounds, such as incisions or eye ablations (LoCascio et al., 2017), were readily repaired in long-term *smedwi-1(RNAi)* animals (Fig. 1D), indicating that the neoblasts are still able to generate the cells that constitute the eye.

Third, we used fluorescent *in situ* hybridization (FISH) on isolated neoblasts to probe potential changes in the lineage biases of the neoblasts (van Wolfswinkel et al., 2014). Using markers of three major classes of neoblasts (epidermal, intestinal and muscle), we found that each of these classes could be readily detected and no significant changes in lineage contributions were found in the *smedwi-1(RNAi)* samples (Fig. 1E).

Fourth, we tested the ability of the neoblasts to respond to injury. Amputations that require tissue replacement trigger a wave of mitosis in the neoblasts around 48 h post-wounding, as well as migration of the neoblasts to the wound site (Wenemoser and Reddien, 2010). When evaluated in small tail amputations, *smedwi-1* animals were indistinguishable from control animals in their ability to mount this mitotic wave, as well as in the distribution of neoblasts through the tissue (Fig. S1F), indicating that neither the ability to cycle nor the ability to migrate was significantly affected. However, in large wound sites (>3 mm width), the density of mitotic cells, as well as the accumulation of neoblasts at the wound site were clearly reduced (Fig. 1F, Fig. S1G). Together, our data indicate that the regeneration defect in *smedwi-1(RNAi)* animals is not caused by loss of neoblast activity or lineage competency, but is related to specific properties of the wound.

SMEDWI-1-depleted tissue fragments display a stalled wound response

The transcriptional response to wounding in *S. mediterranea* has been described in great detail and involves several waves of expression changes that primarily involve the epidermis, the muscle and the neoblasts (Wenemoser et al., 2012; Wurtzel et al., 2015). To determine whether the regeneration defect in *smedwi-1* animals could be due to the inability to mount a wound response, we isolated wound sites at 6 h post-injury for RNA-sequencing analysis and determined expression of annotated wound response genes (Fig. 2A). The induction of many of these wound response genes was clearly detected, and no significant difference in gene expression was observed between the *smedwi-1* wound sites and the controls at this early time point. Over the days after amputation, the expression of wound response genes typically returns to baseline levels, as was indeed observed in control animals. However, in *smedwi-1* animals, the expression of several wound-response genes, including the early growth response genes *egr-2*, *egr-3* and *egr-like-1*, remained elevated for well over 1 week (Fig. 2B). The neoblast wound-response gene *runt-1* also remained elevated until at least day 10 after amputation, whereas general cell cycle-related neoblast genes did reduce their expression levels similar to the progression in wild-type neoblasts (Fig. 2C). Interestingly, positioning genes *wntP-1* and *wntless* also continued to increase in expression over time, instead of dropping back to baseline (Fig. 2D). Together, these data indicate that *smedwi-1(RNAi)* animals correctly initiate the early wound response and are able to activate the genes that are typical for the early phases of regeneration, but are unable to move beyond this stage.

Connective structures are deregulated in *smedwi-1* animals

To elucidate why *smedwi-1* blastemas were unable to progress beyond the initial stages of wound regeneration, we inspected the tissue organization by applying cryosectioning on homeostatic samples and early wound sites. Control homeostatic samples showed a compact epidermal layer, that was tightly connected to a subepidermal layer of collagen (Fig. 2E, Fig. S2E-G). In *smedwi-1* animals, the epidermal layer was noticeably less tight, and more frequently dissociated from the underlying collagen. This phenomenon could already be recognized during fixation, as *smedwi-1* samples had a much higher likelihood of forming blisters or losing the epidermal layer altogether (not shown).

Upon amputation, control wound sites at 6 h post-injury showed early signs of repair, as has been previously reported (Morita and Best, 1974; Pedersen, 1976): while the wound edges remained clearly detectable, the wound surface was rapidly covered by a thin layer of collagen (Fig. 2F), and collagen filaments connecting the edges of the wound were readily observed (Fig. 2G,H). In *smedwi-1* wound sites, deposition of new collagen was still detected, but the collagen layer at the wound was thinner and more fragmented than in controls (Fig. 2F,H). The decrease in collagen in *smedwi-1(RNAi)* animals was confirmed by western blot analysis and levels were found to decrease over the course of several months (Fig. 2I), indicating that this effect builds up over time.

smedwi-1(RNAi) animals misregulate transcripts of epidermal precursor cells

To determine the cause of these structural defects in *smedwi-1* wound sites, we analyzed whether loss of SMEDWI-1 resulted in any changes in the expression of tissue-specific genes (Fig. 3A). While most tissues appeared largely unaffected, we found a strong downregulation of genes specific to late epidermal precursors. We used the sub-classification of epidermal cells into 12 clusters, as established in a previous scRNAseq study (Fincher et al., 2018), to further dissect the cell-type specificity of this change in gene expression (Fig. 3B, Fig. S3A,B). Primarily, genes enriched in epidermal subclusters 4, 7 and 8 were reduced in *smedwi-1* samples. These three clusters are closely related and show high expression of genes that have previously been annotated as ‘category 3 genes’

Development (2025) 152, dev204762. doi:10.1242/dev.204762

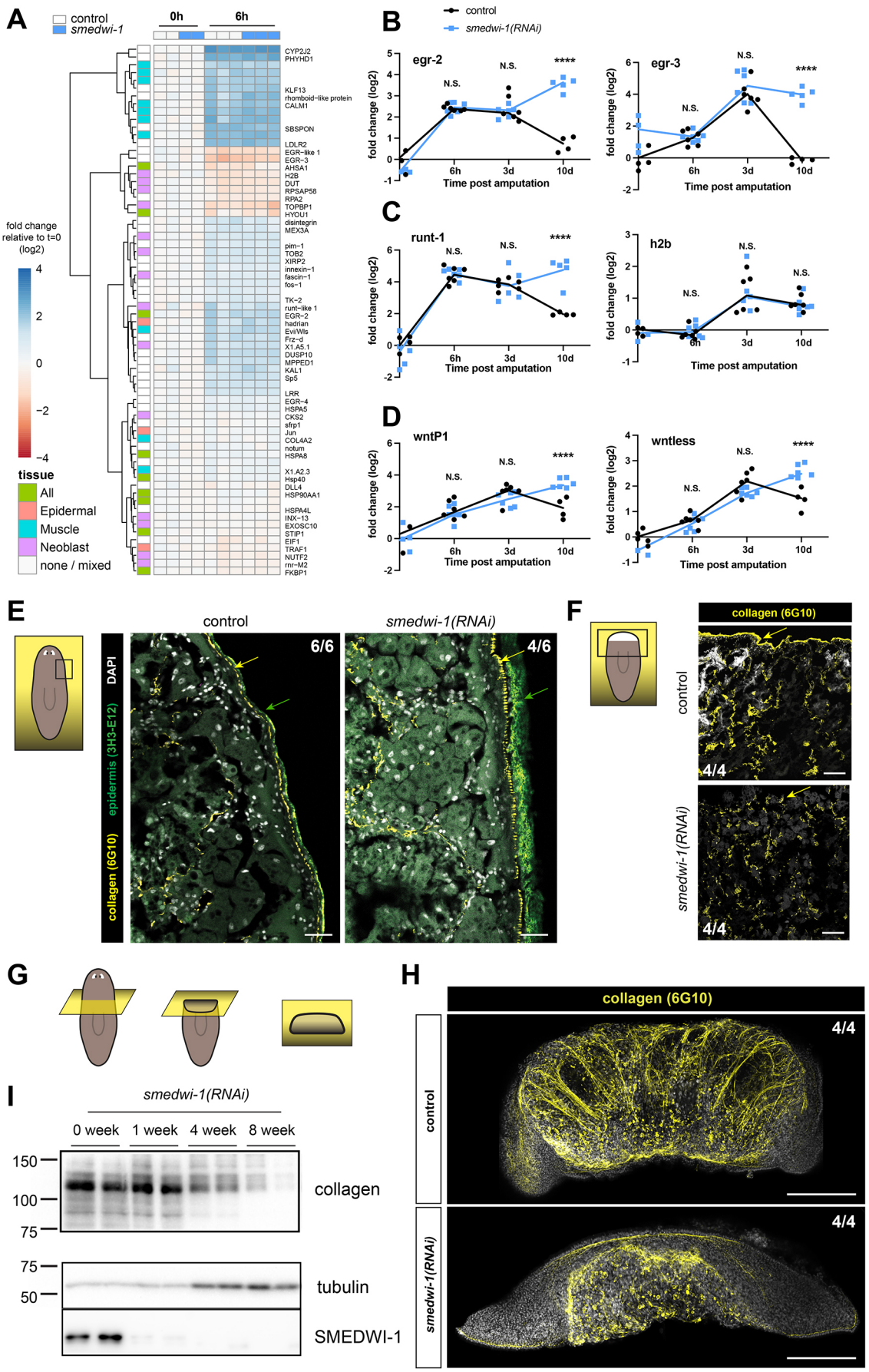

Fig. 2. See next page for legend.

Development (2025) 152, dev204762. doi:10.1242/dev.204762

Fig. 2. Wound response is stalled and collagen is disorganized in *smedwi-1(RNAi)* animals. (A) Heatmap showing the transcript levels (log2 foldchanges relative to averaged 0 h controls as baseline) of previously annotated wound-response genes in control animals and in *smedwi-1(RNAi)* animals at 0 h and 6 h after wounding. For transcripts that are predominantly expressed in one tissue (based on Wurtzel et al., 2015), the tissue is indicated in the left column. Gene names based on best Blast hits to the human proteome are provided unless no significant hit was found. (B-D) qPCR analysis of a timecourse after amputation. Datapoints represent individual biological replicates. Statistical analysis was carried out using an unpaired *t*-test (****P<0.0001; N.S., not significant). (B) Two immediate early genes show the expected increase in expression soon after wounding, but in the absence of SMEDWI-1, the transcript levels remain elevated. (C) Neoblast gene *runt-1*, which is involved in the early wound response, shows the expected increase in expression soon after wounding, but in the absence of SMEDWI-1, the transcript levels remain elevated. The general neoblast transcript *h2b* is not affected by the absence of SMEDWI-1. (D) Two positioning genes show the expected increase in expression soon after wounding, but in the absence of SMEDWI-1, the transcript levels remain elevated. (E) Immunostaining of coronal cryosections of homeostatic *smedwi-1(RNAi)* and control animals shows disorganized collagen at the basement membrane (yellow arrows) and disorganized epidermis (green arrows). Scale bars: 50 µm. (F) Immunostaining of coronal cryosections of *smedwi-1(RNAi)* and control 6 h wound sites shows strong reduction of collagen covering the wound surface (indicated by yellow arrows). Scale bars: 100 µm. (G) Schematic illustrating the plane of view in H. (H) Immunostaining of *smedwi-1(RNAi)* and control animals shows a mesh of collagen in control animals, which is reduced and disorganized after long-term absence of SMEDWI-1. Scale bars: 1 mm. (I) Western blots of homeostatic animals after 1, 4 or 8 weeks of *smedwi-1* knockdown shows the gradual loss of collagen protein from the animals.

(cat3 genes) (Eisenhoffer et al., 2008). They are expressed in cells that are located in the subepidermal layers that frequently have protrusions towards the epidermis (Fig. 3C). Interestingly, markers of early and mature epidermis, as identified in previous studies (van Wolfswinkel et al., 2014; Wurtzel et al., 2017), were not significantly affected (Fig. 3A), indicating that the effect likely involves the lack of expression of the cat3 genes rather than a complete block of the differentiation trajectory in the epidermal lineage. Reduction of several cat3 genes was confirmed by qPCR (Fig. 3D**)**. Furthermore FISH analysis of intact *smedwi-1* animals showed that the RNA level of category gene *agat-3* was indeed reduced and, in particular, was lost from the boundary region, whereas the mature epidermal gene *PRSS12* was not significantly affected (Fig. 3E).

In addition to this stage-specific defect in the epidermal lineage, we observed downregulation of some muscle and cathepsin cell transcripts in the *smedwi-1* samples (Fig. 3A). FISH-based detection of cells expressing the muscle-specific transcript *collagen-2*, as well as immunostaining with the muscle-specific TMUS antibody that labels myosin heavy chain (Cebria et al., 1996) showed that muscle cell density was not reduced in the *smedwi-1* samples (Fig. 3E), supporting the observation that only specific transcripts were affected. However, sub-clustering failed to reveal further cell-type specificity of these gene changes.

We wondered whether the reduction in cat3 epidermal transcripts could be the cause of the *smedwi-1* wound repair defect. From available single cell sequencing data, we found that the transcription factor EGR-5 is specific to the cat3 cells (Fig. S3C), and in agreement with a previous study (Tu et al., 2015), knockdown of EGR-5 resulted in a reduction of transcripts for the cat3 genes, without affecting the levels of transcripts that mark the mature epidermis (Fig. 3F). Interestingly, knockdown of EGR-5 also resulted in a delay in wound closure and failure of regeneration in 40% of large animals (Fig. 3G), mimicking the effect of *smedwi-1* reduction on a shorter timescale. This suggests that reduction of these cat3 transcripts could underlie the *smedwi-1* wound healing phenotype.

Loss of SMEDWI-1 results in destabilization of transcripts for secreted proteins

To determine whether the changes in the transcript levels were the result of transcriptional or post-transcriptional regulation, we performed qPCR for a subset of transcripts, using primers in the mature mRNA as well as in introns, which are only present in the nascent transcript (Fig. 3H). We found that, although levels of mature mRNAs of epidermal genes were decreased, pre-mRNA levels remained largely unaffected, indicating that the effect was on the post-transcriptional level.

SMEDWI-1 is a member of the family of PIWI proteins. These proteins bind small RNAs that can guide the PIWI to RNA targets by sequence complementarity, leading to post-transcriptional regulation of these targets. We thus considered whether the affected epidermal transcripts would be direct targets of SMEDWI-1-bound small RNAs. However, piRNA-mediated regulation typically leads to gene silencing, which is opposite to the effects observed here. Additionally, we found that epidermal sequences were depleted from the SMEDWI-1-bound piRNAs (Fig. S3D). Together, this indicates that the observed effect is unlikely to be a result of piRNA-mediated regulation.

While inspecting the sequences of the destabilized transcripts, we noticed that many of them encoded an N-terminal signal sequence that labels proteins for secretion. We used computational analysis to assign each protein a score for the likelihood of a signal sequence (Hiller et al., 2004), and found that the affected sequences were biased towards secreted proteins (Fig. 3I). Indeed, when we separated the epidermal transcripts into those with and those without a signal sequence, we found that specifically the transcripts of the predicted secreted proteins were affected by loss of SMEDWI-1 (Fig. 3J). Similar results were obtained for the affected transcripts in muscle cells and cathepsin cells (Fig. S3E,F). The production of many of these transcripts (and presumably proteins) specifically in the cat3 cells suggests that these cells function as secretory protein factories in the epidermal lineage.

smedwi-1(RNAi) animals show defects in epidermal secreted structures

The transcripts affected by loss of SMEDWI-1 largely encoded small secreted proteins that did not resemble annotated protein domains by BLAST, and appeared to be specific to planarians. These features fit well with the proposed composition of planarian rhabdoids. Rhabdoids are epidermal rod-shaped granules that characterize the Rhabditophora to which planarians belong, and may be secreted upon stress and injury to assist in physical barrier formation and microbial defense (Hayes, 2017; Smith et al., 1982; Wrona, 1986) (Fig. S4).

To examine the presence of rhabdoids in the epidermis of *smedwi-1(RNAi)* animals, we examined transverse sections stained with Hematoxylin and Eosin (H&E). This confirmed several previously observed phenotypes, including a diminished basement membrane in *smedwi-1(RNAi)* samples (Fig. 4A). Further, the epidermal cells of the *smedwi-1(RNAi)* animals appeared taller than those of control animals, and their structure and contents appeared disorganized. These observations were confirmed by electron microscopy images that, in addition to the diminished basement membrane and disorganized cellular structure, showed a reduction of rhabdoids in the *smedwi-1(RNAi)* epidermal cells (Fig. 4B).

Development (2025) 152, dev204762. doi:10.1242/dev.204762

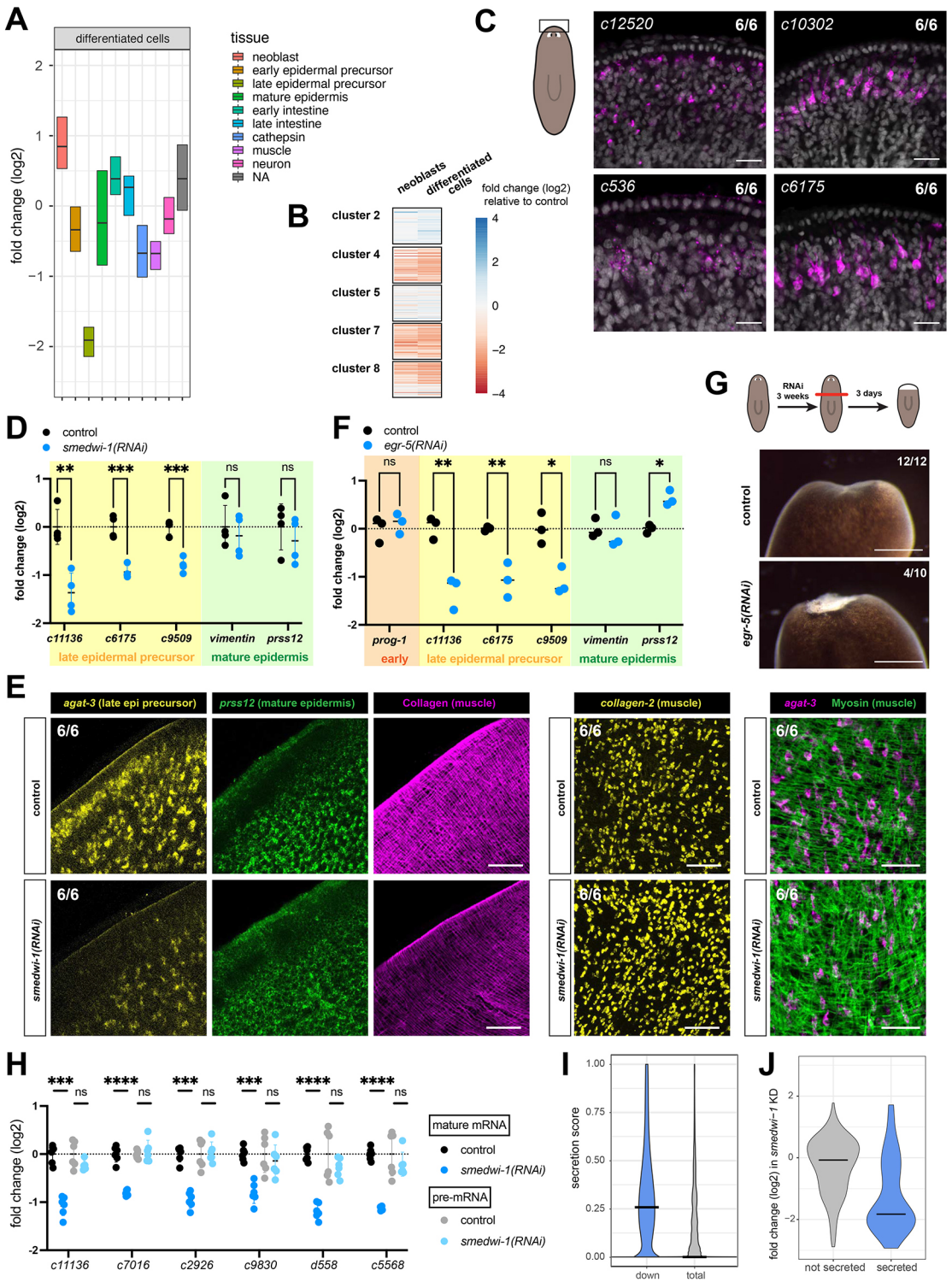

Fig. 3. See next page for legend.

We analyzed the rhabdoids secreted from the planarian epithelium upon salt stress as well as in the mucus trails of control and *smedwi-1(RNAi)* animals. The secretions of control animals contained rhabdoids of around 10 µm long (Fig. 4C), which rapidly inflated and formed a mucous network (Fig. S4A-C). Similar structures were identified in *smedwi-1(RNAi)* secretions, but these rhabdoids disintegrated much faster than control rhabdoids, leading to significantly reduced numbers of recognizable rhabdoids in their mucus trails (Fig. 4C,D). We further found that the control rhabdoids were heavily covered in glycosylated molecules, as detected with the lectin Lens Culinaris Agglutinin (LCA), whereas the *smedwi-1(RNAi)* rhabdoids remained largely unstained (Fig. 4E, Fig. S4C), indicating that their molecular makeup was altered. Together, this indicates that various secreted protein structures were reduced or altered in the *smedwi-1(RNAi)* animals compared to controls.

Development (2025) 152, dev204762. doi:10.1242/dev.204762

Fig. 3. Transcripts downregulated in the absence of SMEDWI-1 predominantly encode secreted proteins. (A) RNAseq analysis of isolated differentiated cells from control and long-term *smedwi-1(RNAi)* animals shows reduced expression of transcripts that are characteristic of epidermal precursors, but not those specific to mature epidermis. Transcripts were assigned to cell types based on single cell RNAseq data (Fincher et al., 2018). (B) Analysis of subclusters of epidermal cells, as identified by Fincher et al. (2018), shows that transcripts reduced in *smedwi-1(RNAi)* animals are largely confined to the clusters that correspond to the late epidermal precursor stage, known as 'category 3 cells'. (C) FISH of several transcripts that are reduced in the *smedwi-1(RNAi)* animals shows the subepidermal localization of the expressing cells. Scale bars: 20 µm. (D) qPCR on independent samples confirms that transcripts of late epidermal precursors, marked by yellow shading, are significantly reduced in long-term *smedwi-1(RNAi)* animals. Mature epidermal transcripts, marked by green shading, remain largely unaltered. Datapoints represent biological replicates (n=4) each consisting of three animals. (E) FISH and immunostaining of *smedwi-1(RNAi)* and control animals shows the presence of muscle cells and mature epidermal cells, but the reduced presence of *agat-3* (in late epidermal precursor cells) and reduced collagen. Scale bars: 50 µm. (F) qPCR analysis of *egr-5(RNAi)* animals shows that transcripts of late epidermal precursors, marked by yellow shading, are significantly reduced. Mature epidermal transcripts, marked by green shading, as well as a characteristic transcript of early epidermal precursors marked by orange shading, remain largely unaltered. Datapoints represent biological replicates (n=3). (G) Live images showing the wound-healing phenotype observed at day 3 after amputation in *egr-5(RNAi)* animals. Scale bars: 1 mm. (H) Quantification of mature mRNA and unspliced pre-mRNA of several affected transcripts by qPCR shows that pre-mRNA levels are unaltered, indicating a post-transcriptional effect. Datapoints represent biological replicates (n=6). (I) Violin plot showing the distribution of predicted signal sequence scores (as determined by the PrediSi package; Hiller et al., 2004) for transcripts reduced in *smedwi-1(RNAi)* animals compared to the whole proteome. (J) Violin plot showing the distribution of fold changes in *smedwi-1(RNAi)* animals relative to controls, of epidermal transcripts encoding secreted and non-secreted proteins. In D, F and H, statistical analysis was carried out using an unpaired *t*-test (*P<0.05; **P<0.01; ***P<0.001; ****P<0.0001; ns, not significant).

smedwi-1(RNAi) animals show defective assembly of the SRP

An important factor in protein secretion is the signal recognition particle (SRP), which is required to efficiently dock ribosomes translating secreted proteins onto the endoplasmic reticulum (ER). SRP consists of several proteins that are connected by the non-coding 7SL RNA (Fig. 5A, Fig. S5A). One side of the complex features SRP54, which binds the signal sequence of the nascent protein and accomplishes the docking of the ribosome on the ER. The other side of the complex consists of SRP9 and SRP14, and is required to arrest translational elongation until the connection to the ER is established. Defects in SRP-mediated relocation of the ribosome activate a quality control mechanism known as regulation of aberrant protein production (RAPP), which leads to degradation of both the protein and the mRNA (Karamyshev et al., 2014). A defect in SRP function therefore could explain the observed reduction in the transcript levels of genes encoding these secreted proteins.

We had previously found that loss of SMEDWI-1 results in the deregulation of many non-coding transcripts in the cells (Allikka Parambil et al., 2024). In agreement with these observations, we detected an increase in the level of the 7SL RNA in *smedwi-1(RNAi)* cells by qPCR (Fig. 5B) as well as by FISH (Fig. 5C, Fig. S5B,C). To determine whether malfunctioning of the SRP complex might underlie the *smedwi-1(RNAi)* phenotype, we knocked down SRP54 and SRP9. Loss of SRP54 resulted in rapid animal death. *srp-9(RNAi)* animals had a mild homeostatic phenotype that involved signs of increased adhesion to the substrate during locomotion. Interestingly, amputation of the *srp-9(RNAi)* animals revealed a penetrant wound regeneration defect that resembled that of the *smedwi-1(RNAi)* animals (Fig. 5D), as well as a similar decrease of rhabdoids in the mucus trails (Fig. S4D,E). Furthermore, loss of SRP9 resulted in a reduction of the mature transcripts of secreted proteins without strong effects on the pre-mRNA levels, similar to the phenotype of *smedwi-1(RNAi)* animals (Fig. 5E).

To evaluate the integrity of the SRP complex in *smedwi-1(RNAi)* animals, we probed the levels of the 7SL RNA and the SRP54 protein (Fig. S5D,E) over the course of the RNAi treatment. Northern blotting confirmed that the 7SL RNA was slightly increased in *smedwi-1(RNAi)* samples (Fig. 5F). On the protein side of the complex, however, we detected a gradual decrease in the level of the SRP54 protein, indicating that in *smedwi-1(RNAi)* animals the stoichiometry of the SRP complex is progressively disrupted.

We next used gel filtration to estimate the size of the SRP complex in control and *smedwi-1(RNAi)* animals (Fig. 5G, Fig. S5F). We detected complexes containing the SRP54 protein around 200 kDa, both in the control animals and in the *smedwi-1(RNAi)* samples. This is in agreement with the expected size of the complex based on its components. SRP54 is the last protein to associate with the complex after other components have already been bound (Grosshans et al., 2001; Politz et al., 2000), and thus the complex containing SRP54 reflects the complete SRP in both conditions. In control samples, the 7SL RNA was found in high molecular weight fractions, as well as in the fractions around 200 kDa, indicating that part of the RNA is present in larger complexes, but a significant fraction is present as part of the complete SRP. In *smedwi-1(RNAi)* samples, however, the 7SL was concentrated in the high molecular weight fractions, suggesting that most of the 7SL RNA was sequestered in high molecular weight (HMW) complexes or aggregates rather than included as part of the mature SRP complex. This is in agreement with the reduced levels of the SRP54 protein that are found in these samples. Together, these data indicate that the SRP complex is progressively disrupted in the *smedwi-1(RNAi)* animals, and that this may underlie the observed alterations in protein secretions, the reduced levels of specific mRNAs, and the wound-healing defects.

Loss of SMEDWI-1 leads to defects in proteostasis and cellular health

Defects in protein secretion could also lead to mislocalization of protein products and the accumulation of protein aggregates in the cells. We wondered whether such defects in proteostasis could be detected in the long-term *smedwi-1(RNAi)* cells.

We used the 6G10 antibody to quantify by western blot the amount of collagen protein that was retained inside cells. Whereas the total levels of collagen were progressively reduced in *smedwi-1(RNAi)* animals (Fig. 2H), we detected an increase in the amount of collagen protein in isolated dissociated cells in the *smedwi-1(RNAi)* samples (Fig. 6A), indicating that some of this protein aberrantly accumulates inside *smedwi-1(RNAi)* cells. Additionally, we detected an increase in ubiquitylated protein in *smedwi-1(RNAi)* samples, indicating that elevated levels of aberrant proteins labeled for degradation are present in these cells (Fig. S6A).

To determine whether the cells respond to this accumulation of retained protein, we used qPCR to determine the expression of several genes involved in retaining proteostasis (Fig. 6B). We found that *smedwi-1(RNAi)* animals expressed significantly increased levels of the cytoplasmic heat-shock protein HSPA8, which is involved in protein maturation and refolding, and of the gene ATG1,

Development (2025) 152, dev204762. doi:10.1242/dev.204762

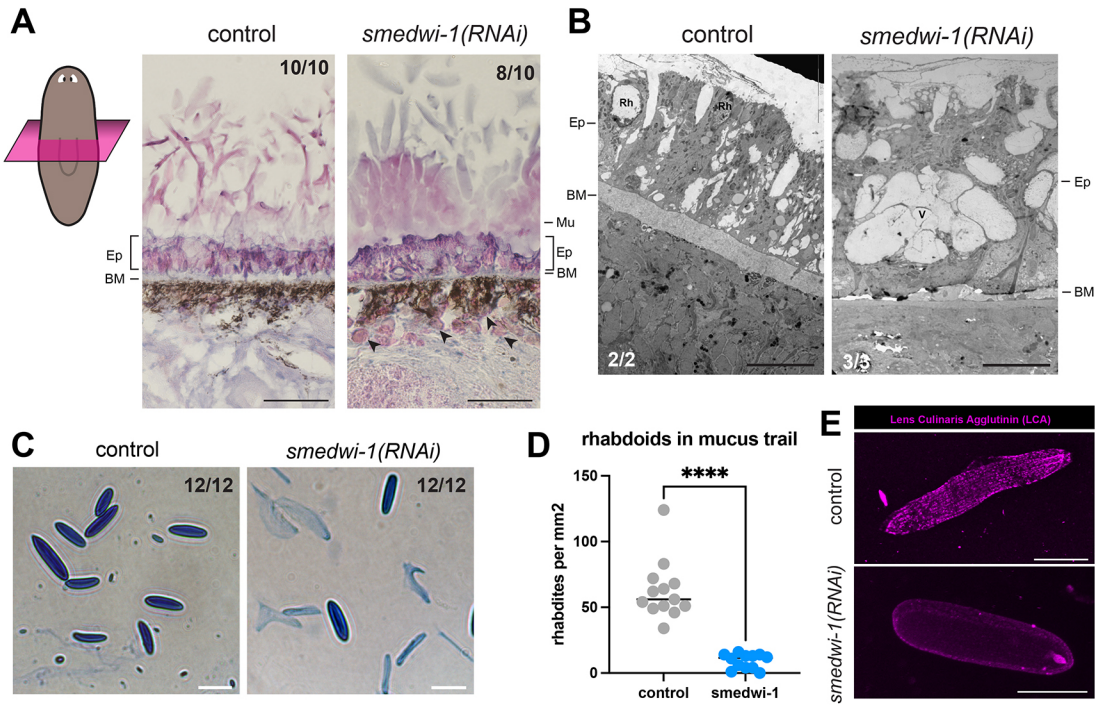

Fig. 4. Secreted structures are affected in *smedwi-1(RNAi)* animals. (A) Transverse sections stained with Hematoxylin and Eosin (H&E) show the altered structure of the epidermis in *smedwi-1(RNAi)* animals, including a less pronounced basement membrane (BM) and sub-epidermal accumulations of material (black arrowheads). Ep, epidermis; Mu, mucus. Scale bars: 50 µm. (B) Electron microscopy confirms the reduction of the basement membrane (BM) in *smedwi-1(RNAi)* animals and the absence of larger oblong rhabdoid structures (Rh). Instead, empty spaces (V) are found in the epidermis (Ep). Scale bars: 10 µm. (C) Anilin Blue staining of rhabdoids as secreted in the mucus trails of control and *smedwi-1(RNAi)* animals. Scale bar: 10 µm. (D) Quantification of the secreted rhabdoids indicates a reduction of rhabdoids in *smedwi-1(RNAi)* trails. Datapoints represent biological replicates (n=12-14). Statistical analysis was carried out using an unpaired t-test (****P<0.0001). (E) Staining of rhabdoids with the rhodamine-coupled lectin LCA shows that the composition of rhabdoids from *smedwi-1(RNAi)* animals is altered. Scale bars: 10 µm.

which is involved in autophagy of aggregates. Further, they also expressed elevated levels of the lysosomal gene β-galactosidase, which is typically upregulated in aged cells with defective proteostasis.

We next investigated whether protein aggregates could be detected in the *smedwi-1(RNAi)* cells. Previously, in the H&E stained samples, we had noticed an increase in large deposits of alkaline material in the subepidermal cells, which could indicate the accumulation of protein (Fig. 4A). We therefore applied the aggregate-specific protein dye Proteostat (Fig. S6B) to analyze the presence of protein aggregates in the epidermal tissues. We found that the *smedwi-1(RNAi)* epidermal cells stained more strongly with this dye than control epidermal cells (Fig. 6C, Fig. S6C). Further, the *smedwi-1(RNAi)* animals had more and larger accumulations of stained material in their subepidermal region, consistent with the presence of deregulated aggregates. Proteostat staining on isolated cells similarly showed aggregates inside the *smedwi-1(RNAi)* cells (Fig. 6D).

To more closely examine the subepidermal cells that were most strongly affected by the protein secretion defect, we used FISH staining for several cat3 transcripts to investigate the morphology of these cells (Fig. 6E). The subepidermal cells that express these transcripts remained present in the *smedwi-1(RNAi)* animals, but the transcript levels were reduced. Interestingly, the cells were also significantly larger and more irregular in shape (Fig. 6F), consistent with accumulation of protein material inside these cells. Similar effects were detected on isolated cells that stained with the cat3 probes (Fig. 6G).

Finally we used TUNEL staining on intact animals to quantify the incidence of cell death. We detected a significant increase in apoptotic cells in the *smedwi-1(RNAi)* animals (Fig. 6H). Apoptotic cells were present throughout the animals, but were notably increased in the subepidermal region (Fig. 6I).

Together, our findings indicate that the deregulation of RNA quality control and alterations in non-coding RNAs, as caused by the absence of SMEDWI-1, can lead to far-reaching consequences that extend to loss of proteostasis, declining health of secretory cells and global defects such as reduced wound repair and accumulation of protein aggregates.

DISCUSSION

Maintaining organismal health over time is a challenging task, as evidenced by the fact that most animals lose their vigor with progressing age, eventually resulting in death. While animals differ significantly in the length of their expected life, the latter part of their lifespan is typically plagued by a remarkably stereotypical set of phenotypes, such as impaired function of muscle and connective tissue, increased susceptibility to infection and impeded wound repair (Ashcroft et al., 2002; López-Otín et al., 2013, 2023). Changes in the efficiency of fundamental molecular processes likely underlie these degenerative phenomena, and indeed many aspects of the central dogma of gene expression are altered with age (López-Otín et al., 2013). Compared to their youthful counterparts, the chromatin of aged cells shows less distinction between accessible and silenced regions (Emerson and Lee, 2023; Yang et al., 2023). The transcription of repetitive regions that are kept suppressed in young cells becomes more pervasive in older cells (Ham et al., 2022; Pabis et al., 2024), leading to higher levels of transposon transcripts, and potentially to novel transposon insertions and genomic instability (Wood and

Development (2025) 152, dev204762. doi:10.1242/dev.204762

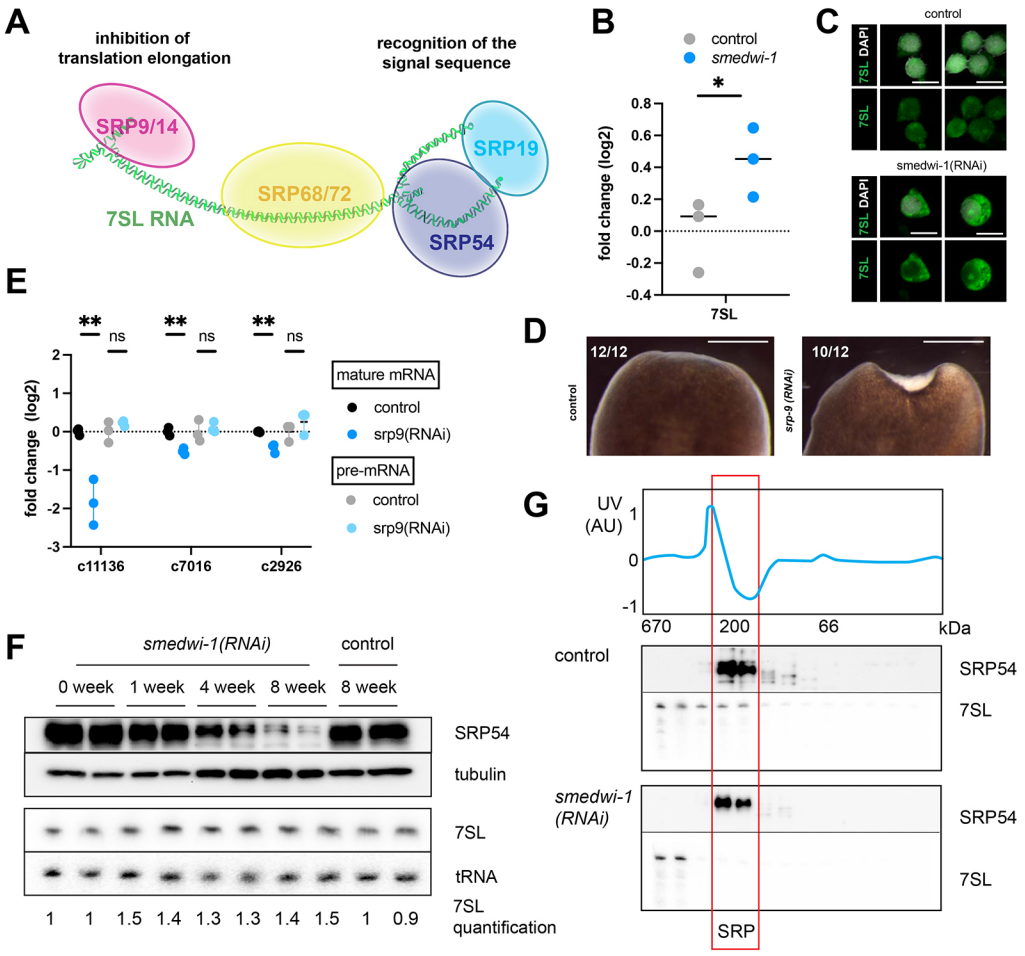

Fig. 5. Absence of SMEDWI-1 leads to deregulation of the signal recognition particle. (A) Schematic showing the composition of the signal recognition particle (SRP), indicating the 7SL RNA (green) as a scaffold that connects the SRP proteins. (B) qPCR data showing the increase in 7SL RNA in the absence of SMEDWI-1. Datapoints represent individual biological replicates (n=3). Statistical analysis was carried out using an unpaired t-test (*P<0.05). (C) RNA FISH for the *7SL* RNA on isolated cells shows increased intensity and prominent accumulation of the RNA in the cytoplasmic space in *smedwi-1(RNAi)* samples compared to controls. Scale bars: 10 µm. (D) Live images showing the wound-healing phenotype observed at day 3 after amputation of *srp-9(RNAi)* animals. Scale bars: 1 mm. (E) Quantification of levels of mature mRNA and unspliced pre-mRNA of several cat3 transcripts by qPCR shows that mature mRNA levels are reduced in the absence of SRP-9, whereas pre-mRNA levels remain unaltered, mimicking the effect of loss of SMEDWI-1. Datapoints represent biological replicates (n=3). Statistical analysis was carried out using an unpaired t-test (**P<0.01; ns, not significant). (F) Western blots and northern blots of animals after 1, 4 or 8 weeks of *smedwi-1* knockdown shows the mild increase of 7SL RNA, and the gradual loss of SRP54 protein from the animals, suggesting disruption of the SRP complex. Numbers below the northern blots indicate relative intensity of the 7SL band compared to the intensity of the tRNA band, as measured using the ImageQuant software. (G) Western blot and northern blot analysis of size fraction samples shows that only a minor fraction of 7SL RNA is found as part of the SRP complex in the *smedwi-1(RNAi)* animals.

Helfand, 2013). Further, proteostasis is altered between young cells and old cells: older cells tend to accumulate protein aggregates, which may impair the functioning of the cells (Huang et al., 2019; Taylor and Dillin, 2011; Walther et al., 2015). Whether these age-associated phenomena are interdependent, and which of them are causal to the downstream macroscopic phenotypes has been difficult to dissect, as the deregulation of these processes occurs concomitantly.

The planarian *Schmidtea mediterranea* normally has an indefinite lifespan and retains its ability to recover from any injuries. Yet here we find that, in the absence of the PIWI protein SMEDWI-1, planarians progressively lose their ability to regenerate and become increasingly fragile. This process takes place over multiple months after the elimination of the SMEDWI-1 protein is already complete, suggesting that this represents a progressive degenerative process, just like aging. Remarkably, the phenotypes that develop in these long-term *smedwi-1(RNAi)* animals also show resemblance to the phenotypes commonly observed in aging animals: we find defects in wound healing, increased sensitivity to microbial exposure, alterations in protein secretion and ECM, accumulation of protein aggregates, and increased apoptosis – all of which are frequently found in aging systems.

We traced the progressive loss of regenerative ability in the *smedwi-1(RNAi)* animals to a defect in protein secretion. We found that loss of the RNA quality control mechanism spearheaded by SMEDWI-1 leads to uncontrolled accumulation of the 7SL RNA, causing misassembly of the SRP, which is essential for co-translational sorting of secreted proteins (Fig. 7A). Secreted proteins are essential for the formation of ECM, and play a particularly important role in epidermal protection and wound healing. The deregulation of protein secretion thus makes the animals less able to close wounds and regenerate, and more susceptible to environmental microbes. We find evidence that, in addition to a reduction in secreted protein, the dysfunction of the SRP also leads to accumulation of such proteins inside cells, which

Development (2025) 152, dev204762. doi:10.1242/dev.204762

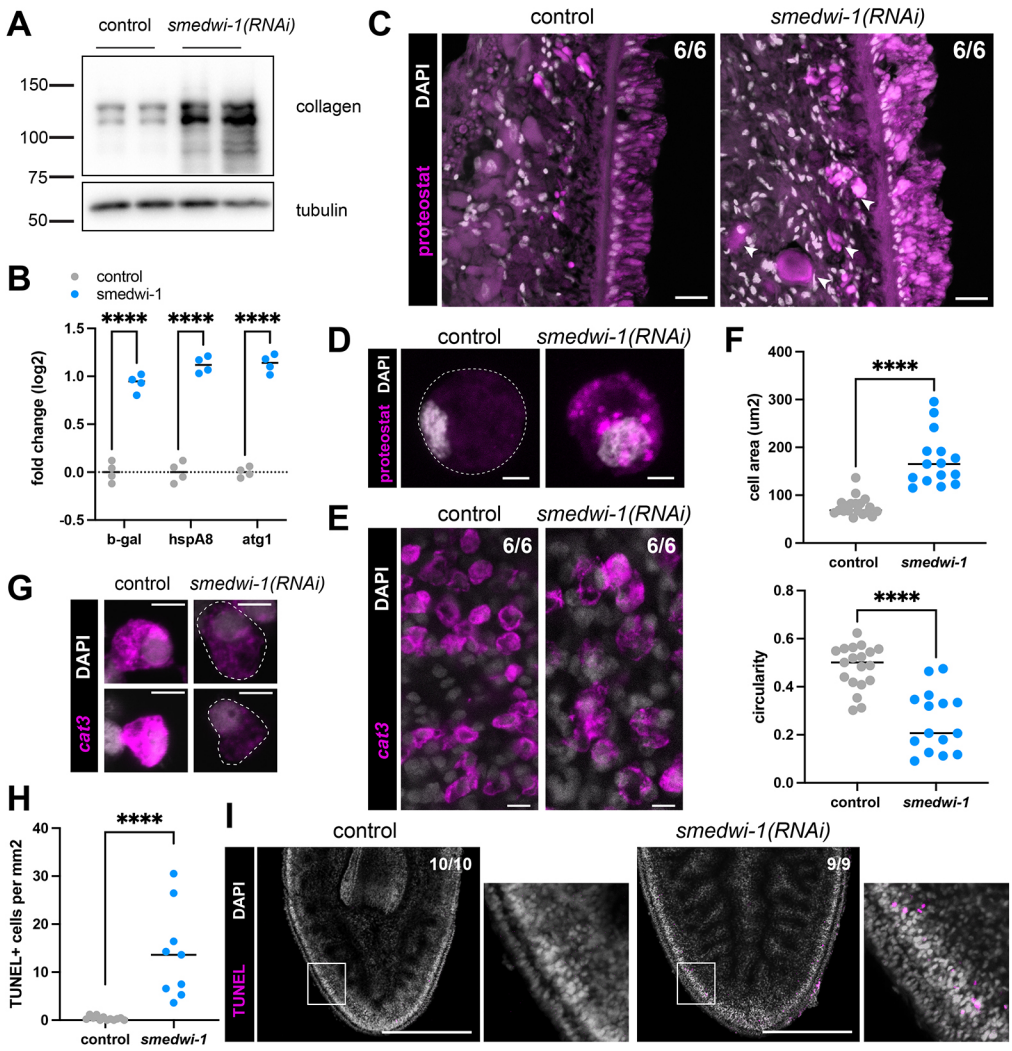

Fig. 6. Proteostasis becomes deregulated in the absence of SMEDWI-1. (A) Western blot of collagen on isolated live cells shows an increase of intracellular collagen in the *smedwi-1(RNAi)* samples. (B) qPCR data showing the increase in several proteostasis-related transcripts in *smedwi-1(RNAi)* samples. Datapoints represent biological replicates (n=4). Statistical analysis was carried out using an unpaired t-test (****P<0.0001). (C) Transverse sections stained with the aggregate-specific protein dye proteostat show the presence of protein accumulations in *smedwi-1(RNAi)* animals, in the epidermal cells and the subepidermal space (arrowheads). Scale bars: 20 µm. (D) Isolated cells stained with the aggregate-specific protein dye proteostat similarly show that *smedwi-1(RNAi)* cells contain aggregates within their cytoplasm. 2D projections of a z-stack through the entire cell are shown. Scale bars: 5 µm. (E) FISH for the cat3 transcript c6175 shows a lower transcript level and altered morphology of the expressing cells in *smedwi-1(RNAi)* samples compared to controls. Scale bars: 10 µm. (F) Quantification of the morphology of the cat3 cells based on the c6175 and c9509 FISH staining shows that, in *smedwi-1(RNAi)* samples, these cells are larger (top) and less regular in shape (bottom) than in controls. Datapoints represent individual cells (n=15-20). Statistical analysis was carried out using an unpaired t-test (****P<0.0001). (G) Isolated cells stained with RNA probes for cat3 genes based c6175 and c9509 similarly show that *smedwi-1(RNAi)* cat3 cells are more weakly stained, larger and less circular than cat3 cells from control samples. Scale bars: 10 µm. (H) Quantification of the density of apoptotic cells, as detected by TUNEL staining in homeostatic asexual animals shows a significant increase in cell death in *smedwi-1(RNAi)* compared to controls. Statistical analysis was carried out using an unpaired t-test (****P<0.0001). (I) TUNEL staining shows increased numbers of apoptotic bodies in *smedwi-1(RNAi)* animals. Apoptotic cells are primarily located in the subepidermal space (areas outlined are shown in the images to their right). Scale bars: 300 µm.

presents as aberrations in cell shape of secretory cells and formation of proteins aggregates (Fig. 7B). It is plausible that proteins that accumulate in the wrong cellular location are more likely to form aggregates; a recent study indeed found that secreted proteins and membrane proteins were major contributors to protein aggregates in aged cells (Chen et al., 2024).

While deregulation of chromatin and proteostasis have frequently been associated with aging cells and are part of the hallmarks of aging (López-Otín et al., 2013, 2023), RNA regulation is not typically evaluated in this context. To our knowledge, our findings form the first indication that defects in protein homeostasis with age could actually (in part) derive from deregulation of RNA quality control, rather than from defects in protein-based mechanisms such as protein folding or autophagy. Notably, in several other systems, aging has been found to coincide with the accumulation of aberrant RNA (Adusumalli et al., 2019; Angelidis et al., 2019; Debès et al., 2023; Enge et al., 2017; Heintz et al., 2017; Kato et al., 2011; Kwon et al., 2023; Wang et al., 2020), indicating that this could be a widespread effect in aging systems.

Remarkably, a similar set of genes to the ones we found downregulated in *smedwi-1(RNAi)* animals has been reported to be downregulated upon the loss of the planarian cytoplasmic

Development (2025) 152, dev204762. doi:10.1242/dev.204762

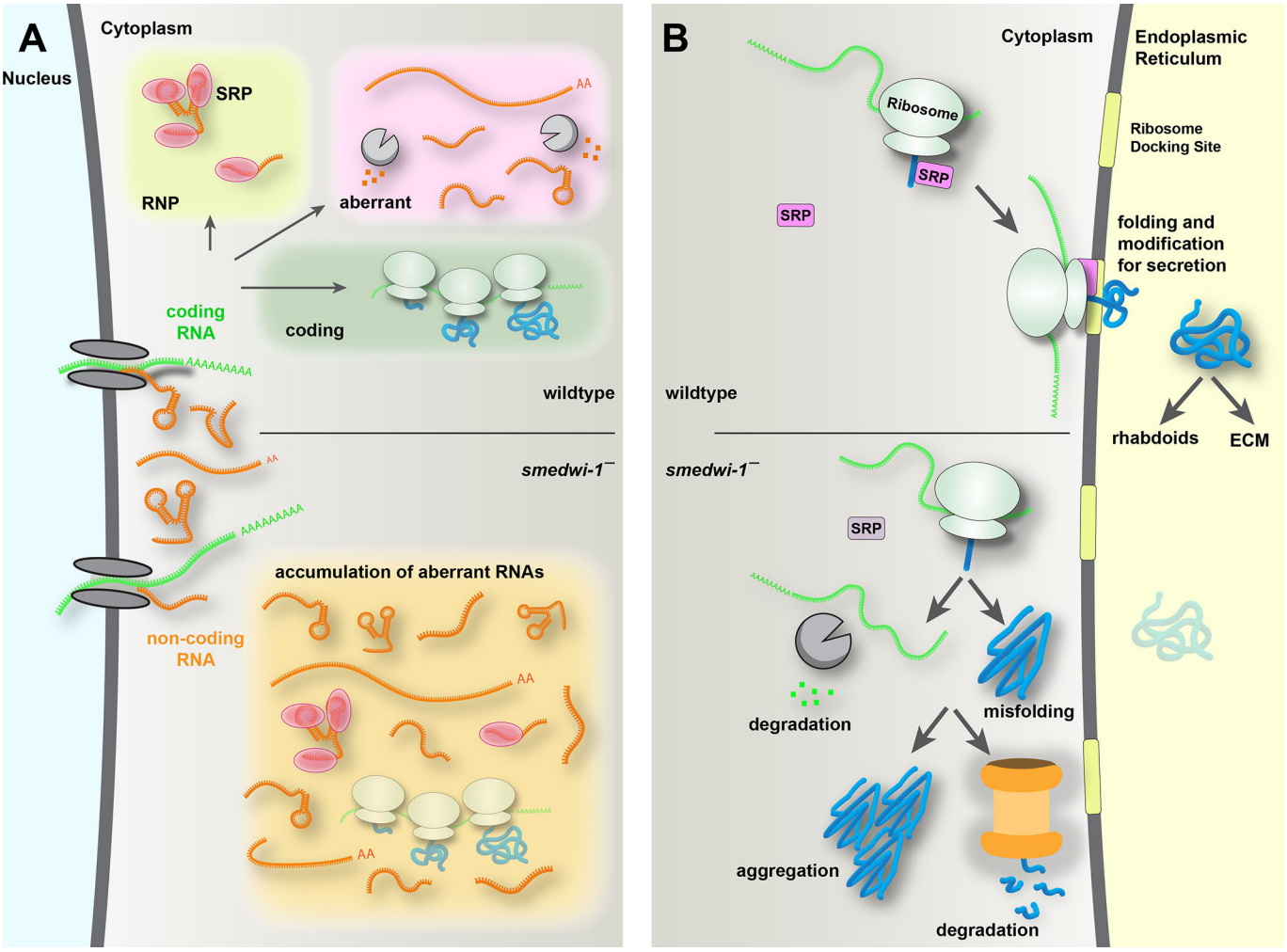

Fig. 7. Model for the gradual loss of cellular health in the absence of SMEDWI-1. (A) In wild-type stem cells, transcripts that are not coding or are mis-assembled with protein co-factors are routinely recognized and degraded. In the absence of SMEDWI-1, this selection process is defective, and aberrant RNAs can accumulate in the cells. Over time, this leads to a reduction in correctly assembled ribonuclear protein complexes (RNPs) such as the signal recognition particle (SRP). (B) The SRP functions to guide ribosomes that translate secreted proteins to the endoplasmic reticulum to continue protein translation and allow for appropriate folding and transport of the protein product. If such a ribosome is not correctly relocated, the protein product is released in the cytoplasm and marked for degradation together with the mRNA that produced it. Alternatively, the protein product may escape degradation and accumulate in the cytoplasm as a protein that is prone to misfolding and aggregation.

polyA-binding protein PABPC (Bansal et al., 2017). When comparing these two datasets, we found that specifically the transcripts encoding secreted proteins characteristic of the late epidermal precursor stage are reduced in the RNAseq data of both *smedwi-1(RNAi)* and *pabpc(RNAi)* samples (Fig. S6D). In addition, a regeneration phenotype and a prolonged wound response similar to those found in *smedwi-1(RNAi)* have been reported for *pabpc(RNAi)* animals, suggesting that these phenotypes may well be related. It is possible that PABPC is required for the stability of the mRNAs for these secreted proteins, or that it otherwise assists in the direction of these transcripts to the SRP and the ER-coupled translation. Alternatively, the loss of PABPC may result in broader anomalies in RNA control mechanisms that extend to non-coding RNAs and RNPs.

PIWI proteins are present in long-lived cells in a wide range of contexts. They are best known for their presence in the germline, but are also maintained in the long-lived stem cells of all studied highly regenerative animals (van Wolfswinkel, 2014), as well as in mesenchymal and hematopoietic stem cells in mammals (Sharma et al., 2001; Wu et al., 2010). Interestingly, PIWI proteins have also been detected in neurons, which are some of the most long-lived post-mitotic cells (Nandi et al., 2016; Perrat et al., 2013; Rajasethupathy et al., 2012). It is possible that, in addition to their well-known role in transposon control, PIWI proteins function to maintain RNA health in each of these cell types and thereby mediate the longevity of these systems.

The PIWI protein SMEDWI-1 was one of the first genes identified as enriched in the planarian stem cells (Reddien et al., 2005). It has been widely used as a stem cell marker, but its role in planarian biology remained unclear as elimination of SMEDWI-1 did not result in a direct organismal phenotype. We now propose that it is exactly this lifelong presence of SMEDWI-1 in the neoblasts that bestows the neoblasts, and with them the planarians, their unusually long lifespan and regenerative abilities. SMEDWI-1 is not essential for the direct maintenance or replicative abilities of the stem cells, but it safeguards the RNA health of these cells and their descendants, thereby maintaining their lifelong functionality. Based on our findings we propose that, without SMEDWI-1, the planarians would become mere mortals, similar to

Development (2025) 152, dev204762. doi:10.1242/dev.204762

most other animals, and would probably experience similar age-related decline.

Study limitations

This study focused on defects in the SRP in the *smedwi-1(RNAi)* animals, but it is possible that other RNPs are also affected by the deregulation of RNA control in the absence of SMEDWI-1. Misassembly of various RNPs may contribute to the decay in cellular health in these animals and may deregulate the intercellular communication to the stem cells, which could add to the misregulation of regeneration. Further, the mechanism by which loss of SMEDWI-1 causes the accumulation of aberrant RNA has not been resolved in this study.

The rod-shaped structures secreted from the planarian epidermis are a heterogenous set of granules. We were not able to conclusively determine that they would all fall under the term 'rhabdites' and thus chose to refer to them as rhabdite-like structures or 'rhabdoids'.

The exact epitope of the 6G10 antibody remains unknown. Based on our data, the most likely target is a collagen, and we have interpreted the labeling accordingly.

MATERIALS AND METHODS

Animal husbandry

Schmidtea mediterranea asexual clonal strain ClW4 and sexual strain S2 were maintained as previously described (Newmark and Sánchez Alvarado, 2000). Briefly, animals were cultured in 1× Montjuic salts at 20°C, fed homogenized beef liver paste every 1-2 weeks, and expanded through continuous cycles of amputation or fissioning and regeneration. Animals were starved 1-2 weeks prior to experiments. During RNAi experiments, animals were maintained in water supplemented with gentamycin to prevent bacterial growth. Experiments in this manuscript were performed on sexual animals, except where explicitly indicated that asexuals were used.

RNAi

Regions of planarian genes 0.5-2 kb in length were amplified from complementary DNA (cDNA) using sequence-specific primers (Table S1) with adaptor sequences. The PCR product was cloned into the pGEM-T vector (Promega) and verified by Sanger sequencing. Both RNA strands were synthesized *in vitro* from PCR-generated forward and reverse templates with flanking T7 promoters (TAATACGACTCACTATAGG), and annealed by incubation at 37°C for 30 min. The transcribed ssRNA as well as the final dsRNA product were verified by gel electrophoresis.

Animals were starved 1-2 weeks prior to RNAi experiments. RNAi food was prepared by mixing 2 µl of generic food coloring, 2 µl of dsRNA and 50 µl of homogenized beef liver (Rouhana et al., 2013) and fed to animals in 3-day intervals for a total of five feeds unless noted otherwise. DsRNA matching *C. elegans* gene *unc-22* was used as a negative control.

Whole-mount fluorescent *in situ* hybridization and immunofluorescence

Fixations, whole-mount *in situ* hybridization (ISH) and immunofluorescence were performed as previously described (Pearson et al., 2009), with alterations described by King and Newmark (2013). Briefly, formaldehyde fixed animals were bleached using formamide bleach solution and treated with proteinase K (2 µg/ml) in PBSTx. For FISH, following overnight hybridization at 56°C, samples were washed sequentially in pre-hyb solution, 1:1 pre-hyb-2×SSC, 2×SSC and 0.2×SSC at 56°C. Probes were detected with anti-DIG-POD (Roche, 11207733910), anti-Fl-POD (Roche, 11426346910) or anti-DNP-HRP (Perkin Elmer, PF1129). After tyramide development (King and Newmark, 2013), peroxidase was inactivated by incubation in 1% sodium azide. Specimens were counterstained with DAPI (Sigma). For immunofluorescence, animals were blocked and incubated with primary antibody overnight, followed by incubation with goat anti-rabbit IgG HRP conjugate (Life Technologies) or goat anti-mouse IgG HRP conjugate (Life Technologies). Primary antibodies used were rabbit anti-phospho-Histone3[Ser10] (Millipore, clone 63-1C-8; 1:750), mouse anti-collagen 6G10 (DHSB, Ross et al., 2015; 1:500), mouse epidermal antibody 3H3 (DHSB, Forsthoefel et al., 2014; 1:100) and mouse anti-myosin antibody TMUS (Cebria et al., 1996; 1:50). Signals were developed using Tyramide SuperBoost Kits (Invitrogen).

Cyrosectioning and electron microscopy

For immunostaining, animals were fixed in 4% formaldehyde, followed by a dehydration series from 2% to 25% sucrose, and embedding in OCT (Tissue-Tek, Sakura). Sections were cut at 20 µm using a cryostat (Leica). Antibody incubations were performed as described above for whole mounts.

For H&E staining and electron microscopy (EM), animals were processed as described by Brubacher et al. (2014). Briefly, animals were fixed in fixative containing 2% formaldehyde, 2.5% glutaraldehyde, 54.2 mM cacodylate and 0.78 mM $CaCl_2$. Samples were then transferred to the EM facility or, for H&E staining, dehydrated in sucrose and embedded in OCT (Tissue-Tek, Sakura).

Proteostat staining was performed by incubation with a 1:1000 dilution of the dye in PBS for 10 min at room temperature followed by a 20 min destaining in 1% acetic acid (Shen et al., 2011). MG132 treatment (proteasome inhibitor for Proteostat control) was performed by soaking animals for 16 h in 1% DMSO in the presence of 100 µM MG132.

Rhabdoid isolation and staining

For quantification of rhabdoids in mucus trails, five animals were left to roam in a 3 cm dish for 2 h. After removing the animals, the mucus left in the dish was stained in 5% Aniline Blue in PBS for 10 min, rinsed in PBS and imaged immediately for counting.

Images of rhabdoids were obtained by placing an individual animal on a microscope slide, removing remaining water and adding 20 µl 5 M NaCl. After 10 s, the animal was removed, and the secreted rhabdoids were stained by addition of 2 µl 5% Aniline Blue or 1% Lens Culinaris Agglutinin coupled to Rhodamine (Vector Systems) and covered with a coverslip. Samples were imaged immediately.

Neoblast isolation and staining

Neoblasts in G2/M phase (X1) and differentiated cells (Xins) were isolated by fluorescence-activated cell sorting based on DNA content (Hoechst fluorescence), as reported by Hayashi et al. (2006), following procedures described previously (van Wolfswinkel et al., 2014).

For staining of the isolated cells, cell suspensions isolated by FACS were collected in CMFB and centrifuged at ∼300 ***g*** for 5 min at 4°C. Cells were washed in CMF, spotted onto poly-D-lysine-coated coverslips (BD Biosciences), allowed to settle for ∼30 min, and fixed in 4% PFA (in PBS) for 20 min at room temperature. Controls and treatment were always spotted on the same cover slip, and went through all staining steps in the same well. Immunofluorescence and FISH labeling were carried out similarly to the whole-mount protocol, with wash steps and antibody incubations shortened to 10 min and 1 h, respectively.

Microscopy and image analysis

Images were taken on a Zeiss LSM800 confocal microscope. Control and RNAi animals were imaged with the same magnification, laser intensity and gain, at comparable anatomical position. Cell counting and quantification of fluorescence intensity were performed in Fiji (Schindelin et al., 2012). Quantification size and circularity of secretory cells was performed in PIQ (Allikka Parambil et al., 2024) using 2D images.

qPCR analysis

Total RNA was isolated by Trizol and quantified by Qubit. To distinguish between changes in global RNA level or in level of polyadenylation, two cDNA preparations were synthesized from the same RNA samples: one primed by hexamers and one primed by oligo dT. For all cDNA preparations, ProtoScriptII (NEB) was used according to the manufacturer instructions, using 1 µg RNA as starting material in a 20 µl reaction. cDNA was diluted 1:5 in MilliQ water and 1 µl was applied to a 10 µl qPCR reaction using EvaGreen mastermix (Biotium). Primers are listed in Table S1. RT and qPCR reactions of samples and controls were run in parallel in the same plates. qPCRs were run on a QuantStudio 3 instrument

Development (2025) 152, dev204762. doi:10.1242/dev.204762

(ABI) with the following program: 95°C for 20 s; 40 cycles of 95°C for 5 s; 60°C for 20 s; followed by a melting curve analysis.

RNA-seq library generation

For mRNA-seq libraries of neoblasts and differentiated cells, or regenerating tissue, large animals were fed control *unc-22* or *smedwi-1* dsRNA in liver for 2 months before FACS sorting or amputation. RNA was extracted from isolated tissues using TRIzol Reagent (Invitrogen), and libraries were generated using TruSeq RNA Library Prep Kit v2 (Illumina) following the manufacturer's instructions.

Processing of mRNA-seq data

mRNA libraries were sequenced on a NovaSeq (Illumina). Additionally, previously generated data available under SRA accession number PRJNA905109 was included in the analyses. Reads were mapped against *Schmidtea mediterranea* transcriptomes WIX1 (van Wolfswinkel et al., 2014), dd_Smed_v6 (Liu et al., 2013) or unigene (Robb et al., 2015) using Bowtie2 (Langmead and Salzberg, 2012), and further processed with SAMtools (Li et al., 2009). For transposon expression analysis, reads were mapped against the *Schmidtea mediterranea* SMESG.1 genome (Grohme et al., 2018) using STAR (Dobin et al., 2013).

Processing of small RNA-seq data

Small RNA libraries were reprocessed from (Allikka Parambil et al., 2024). Following adaptor trimming by Cutadapt (Martin, 2011), reads were mapped against the *Schmidtea mediterranea* SMESG.1 genome using Bowtie (Langmead, 2010), allowing for two mismatches and up to 20 mapping locations. The reads are then counted strand-sensitively toward exons of transcripts or transposon copies using BEDTools.

Signal sequence prediction

The total *Schmidtea mediterranea* transcriptome was translated using ORFFinder (NCBI) to obtain a total proteome. The likelihood of a signal sequence in each protein was predicted using PrediSi (Hiller et al., 2004) (http://www.predisi.de/home.html), using default parameters. PrediSi calculates a normalized score on a scale between 0 and 1 for each protein sequence. A score greater than 0.5 means that the examined sequence likely contains a signal peptide. This was found in less than 5% of the planarian protein sequences.

Size fractionation

Animals were rinsed in FPLC buffer (10 mM Tris (pH 7.5), 150 mM NaCl, 5 mM $MgCl_2$, 2 mM DTT, 0.2% NP-40 and 5% glycerol), and frozen in liquid nitrogen. After grinding and douncing, lysates were centrifuged at 20,000 ***g*** for 10 min. Supernatant was supplemented with RNase inhibitor and protease inhibitor cocktail (Complete, Roche), and 300 µl was loaded onto a Superdex 200 column (300/10, Cytiva) using a 1 ml loop on an AKTA Pure system. The column was calibrated with thyroglobulin (670 kDa), apoferritin (430 kDa), β-amylase (200 kDa), bovine serum albumin (66 kDa) and (to mark the total column volume) acetone (0 kDa). Fractions were collected after the void until the end of the column volume.

For analysis of protein content, each fraction was combined with sample buffer and loaded on a 12% protein gel. For analysis of RNA content, each fraction was supplemented with 1% SDS and an equal volume of acid PCI (phenol-chloroform-isoamylalcohol). The RNA in the aquatic phase was precipitated with 3 volumes of ethanol and 1 µl glycoblue.

SDS-PAGE and western blotting

Individual 1-3 mm sized animals were homogenized in protein loading buffer (60 mM Tris-Cl at pH6.8, 5% glycerol, 1% SDS and 2.5% β-mercaptoethanol) and separated on 8% denaturing polyacrylamide gel. Samples were transferred to PVDF membrane, blocked and incubated with the primary antibody followed by secondary antibody, in PBSTw containing 1.5% milk. For the detection of ubiquitin, blots were denatured (6 M guanidinium chloride, 20 mM Tris at pH 7.5, 1 mM PMSF and 5 mM β-mercaptoethanol for 30 min) prior to blocking. The following antibodies were used: mouse anti-α-tubulin (MABT205, Millipore) at 1:10000; rabbit anti-SMEDWI-1 (Allikka Parambil et al., 2024) at 1:2000; mouse anti-collagen (6G10, DHSB; Ross et al., 2015) at 1:1000-2000; rabbit anti-SRP54 (orb25807, Biorbyt) at 1:1000; mouse anti-myosin antibody TMUS (Cebria et al., 1996) at 1:500; rabbit anti-ubiquitin (P37, Cell Signaling Technology) at 1:300; goat anti-rabbit IgG HRP conjugate (Life Technologies) at 1:10,000; and goat anti-mouse IgG HRP conjugate (Life Technologies) at 1:10,000.

Northern blotting

Samples were diluted with RNA loading dye (NEB) and separated on a 12% acrylamide gel. Gels were blotted to Hybond N+ membrane using a semidry apparatus (BioRad). Membranes were crosslinked at 12,000 J/cm^2 using a UV crosslinker (UVP), and incubated in ExpressHyb (Takara) containing end-labeled probe overnight at 42°C. After washes in 2×SSC with 0.05% SDS and 0.1×SSC with 0.1%SDS, membranes were exposed on a phosphoimager screen. Screens were read on a GE Typhoon FLA 9000 gel imager, and quantified using the imageQuant software.

Probes were ordered as DNA oligos and were end-labeled using gamma-ATP and PNK (NEB) for 1 h at 37°C. End-labeled probes were cleaned up using a G25 column (Zymo) before use for hybridization. Probe sequences are listed in Table S1.

Quantification and statistical analysis

In all experiments shown, datapoints represent biological replicates. Mean values are indicated by a horizontal bar. Levels of significance were calculated with unpaired two-tailed Student's *t*-test, using the Prism software package unless otherwise indicated. Analysis of genome-wide data was carried out as described above.

Acknowledgements

We thank the Keck DNA Sequencing Facility at Yale for Illumina sequencing, and the Center for Cellular and Molecular Imaging (CCMI) for electron microscopy of our samples. We further acknowledge the Yale Science Hill Imaging Facility and the Science Hill FACS Facility for providing access to confocal microscopes, cryostat and FACS equipment. We are grateful to Francesc Cebria for sharing the TMUS antibody. We thank members of the Van Wolfswinkel Lab for discussion and comments.

Competing interests

The authors declare no competing or financial interests.

Author contributions

Conceptualization: M.Z., D.L., J.C.v.W.; Formal analysis: M.Z., D.L., A.P., J.C.v.W.; Funding acquisition: J.C.v.W.; Investigation: M.Z., D.L., S.A.P., K.M., K.D., J.C.v.W.; Methodology: D.L., A.V., A.P.; Software: A.P.; Supervision: J.C.v.W.; Visualization: A.P.; Writing – original draft: J.C.v.W.; Writing – review & editing: M.Z., D.L., A.V., S.A.P., A.P.

Funding

This work was supported by the National Institutes of Health (R35GM158281 and R01AG078926) and by the Vallee Foundation. Open Access funding provided by Yale University. Deposited in PMC for immediate release.

Data and resource availability

Sequencing data generated in the course of this study have been deposited in the SRA under accession number PRJNA1209026. All other relevant data and details of resources can be found within the article and its supplementary information.

Peer review history

The peer review history is available online at https://journals.biologists.com/dev/lookup/doi/10.1242/dev.204762.reviewer-comments.pdf

References

Adusumalli, S., Ngian, Z. K., Lin, W. Q., Benoukraf, T. and Ong, C. T. (2019). Increased intron retention is a post-transcriptional signature associated with progressive aging and Alzheimer's disease. *Aging Cell* **18**, e12928. doi:10.1111/acel.12928

Allikka Parambil, S., Li, D., Zelko, M., Poulet, A. and van Wolfswinkel, J. C. (2024). piRNA generation is associated with the pioneer round of translation in stem cells. *Nucleic Acids Res.* **52**, 2590-2608. doi:10.1093/nar/gkad1212

Angelidis, I., Simon, L. M., Fernandez, I. E., Strunz, M., Mayr, C. H., Greiffo, F. R., Tsitsiridis, G., Ansari, M., Graf, E., Strom, T.-M. et al. (2019). An atlas of the aging lung mapped by single cell transcriptomics and deep tissue proteomics. *Nat. Commun.* **10**, 963. doi:10.1038/s41467-019-08831-9

Ashcroft, G. S., Mills, S. J. and Ashworth, J. J. (2002). Ageing and wound healing. *Biogerontology* **3**, 337-345. doi:10.1023/A:1021399228395
Bansal, D., Kulkarni, J., Nadahalli, K., Lakshmanan, V., Krishna, S., Sasidharan, V., Geo, J., Dilipkumar, S., Pasricha, R., Gulyani, A. et al. (2017). Cytoplasmic poly (A)-binding protein critically regulates epidermal maintenance and turnover in the planarian Schmidtea mediterranea. *Development* **144**, 3066-3079. doi:10.1242/dev.152942
Brubacher, J. L., Vieira, A. P. and Newmark, P. A. (2014). Preparation of the planarian Schmidtea mediterranea for high-resolution histology and transmission electron microscopy. *Nat. Protoc.* **9**, 661-673. doi:10.1038/nprot.2014.041
Cebria, F., Vispo, M., Bueno, D., Carranza, S., Newmark, P. and Romero, R. (1996). Myosin heavy chain gene in Dugesia (G.) tigrina: a tool for studying muscle regeneration in planarians. *Int. J. Dev. Biol. Suppl.* **1**, 177S-178S.
Chen, Y. R., Harel, I., Singh, P. P., Ziv, I., Moses, E., Goshtchevsky, U., Machado, B. E., Brunet, A. and Jarosz, D. F. (2024). Tissue-specific landscape of protein aggregation and quality control in an aging vertebrate. *Dev. Cell* **59**, 1892-1911.e1813. doi:10.1016/j.devcel.2024.04.014
Czech, B., Munafò, M., Ciabrelli, F., Eastwood, E. L., Fabry, M. H., Kneuss, E. and Hannon, G. J. (2018). piRNA-guided genome defense: from biogenesis to silencing. *Annu. Rev. Genet.* **52**, 131-157. doi:10.1146/annurev-genet-120417-031441
Debès, C., Papadakis, A., Grönke, S., Karalay, Ö., Tain, L. S., Mizi, A., Nakamura, S., Hahn, O., Weigelt, C., Josipovic, N. et al. (2023). Ageing-associated changes in transcriptional elongation influence longevity. *Nature* **616**, 814-821. doi:10.1038/s41586-023-05922-y
Deere, J. A., Holland, P., Aboobaker, A. and Salguero-Gómez, R. (2024). Non-senescent species are not immortal: Stress and decline in two planaria species. *J. Anim. Ecol.* **93**, 1722-1735. doi:10.1111/1365-2656.14184
Dobin, A., Davis, C. A., Schlesinger, F., Drenkow, J., Zaleski, C., Jha, S., Batut, P., Chaisson, M. and Gingeras, T. R. (2013). STAR: ultrafast universal RNA-seq aligner. *Bioinformatics* **29**, 15-21. doi:10.1093/bioinformatics/bts635
Eisenhoffer, G. T., Kang, H. and Sanchez Alvarado, A. (2008). Molecular analysis of stem cells and their descendants during cell turnover and regeneration in the planarian Schmidtea mediterranea. *Cell Stem Cell* **3**, 327-339. doi:10.1016/j.stem.2008.07.002
Emerson, F. J. and Lee, S. S. (2023). Chromatin: the old and young of it. *Front. Mol. Biosci.* **10**, 1270285. doi:10.3389/fmolb.2023.1270285
Enge, M., Arda, H. E., Mignardi, M., Beausang, J., Bottino, R., Kim, S. K. and Quake, S. R. (2017). Single-cell analysis of human pancreas reveals transcriptional signatures of aging and somatic mutation patterns. *Cell* **171**, 321-330.e314. doi:10.1016/j.cell.2017.09.004
Fincher, C. T., Wurtzel, O., De Hoog, T., Kravarik, K. M. and Reddien, P. W. (2018). Cell type transcriptome atlas for the planarian Schmidtea mediterranea. *Science* **360**, eaaq1736. doi:10.1126/science.aaq1736
Forsthoefel, D. J., Waters, F. A. and Newmark, P. A. (2014). Generation of cell type-specific monoclonal antibodies for the planarian and optimization of sample processing for immunolabeling. *BMC Dev. Biol.* **14**, 45. doi:10.1186/s12861-014-0045-6
Gambino, G., Ippolito, C., Modeo, L., Salvetti, A. and Rossi, L. (2020). 5-Fluorouracil-treated planarians, a versatile model system for studying stem cell heterogeneity and tissue aging. *Biol. Cell* **112**, 335-348. doi:10.1111/boc.202000040
Grohme, M. A., Schloissnig, S., Rozanski, A., Pippel, M., Young, G. R., Winkler, S., Brandl, H., Henry, I., Dahl, A., Powell, S. et al. (2018). The genome of Schmidtea mediterranea and the evolution of core cellular mechanisms. *Nature* **554**, 56-61. doi:10.1038/nature25473
Grosshans, H., Deinert, K., Hurt, E. and Simos, G. (2001). Biogenesis of the signal recognition particle (SRP) involves import of SRP proteins into the nucleolus, assembly with the SRP-RNA, and Xpo1p-mediated export. *J. Cell Biol.* **153**, 745-762. doi:10.1083/jcb.153.4.745
Haase, A. D., Ketting, R. F., Lai, E. C., van Rij, R. P., Siomi, M., Svoboda, P., van Wolfswinkel, J. C. and Wu, P.-H. (2024). PIWI-interacting RNAs: who, what, when, where, why, and how. *EMBO J.* **43**, 5335-5339. doi:10.1038/s44318-024-00253-8
Ham, S., Kim, S. S., Park, S., Kim, E. J. E., Kwon, S., Park, H.-E. H., Jung, Y. and Lee, S.-J. V. (2022). Systematic transcriptome analysis associated with physiological and chronological aging in Caenorhabditis elegans. *Genome Res.* **32**, 2003-2014. doi:10.1101/gr.276515.121
Hayashi, T., Asami, M., Higuchi, S., Shibata, N. and Agata, K. (2006). Isolation of planarian X-ray-sensitive stem cells by fluorescence-activated cell sorting. *Dev. Growth Differ.* **48**, 371-380. doi:10.1111/j.1440-169X.2006.00876.x
Hayes, M. J. (2017). Sulphated glycosaminoglycans support an assortment of planarian rhabdite structures. *Biol. Open* **6**, 571-581. doi:10.1242/bio.024554
Heintz, C., Doktor, T. K., Lanjuin, A., Escoubas, C. C., Zhang, Y., Weir, H. J., Dutta, S., Silva-García, C. G., Bruun, G. H., Morantte, I. et al. (2017). Splicing factor 1 modulates dietary restriction and TORC1 pathway longevity in C. elegans. *Nature* **541**, 102-106. doi:10.1038/nature20789
Hiller, K., Grote, A., Scheer, M., Munch, R. and Jahn, D. (2004). PrediSi: prediction of signal peptides and their cleavage positions. *Nucleic Acids Res.* **32**, W375-W379. doi:10.1093/nar/gkh378
Huang, C., Wagner-Valladolid, S., Stephens, A. D., Jung, R., Poudel, C., Sinnige, T., Lechler, M. C., Schlörit, N., Lu, M., Laine, R. F. et al. (2019). Intrinsically aggregation-prone proteins form amyloid-like aggregates and contribute to tissue aging in Caenorhabditis elegans. *eLife* **8**, e43059. doi:10.7554/eLife.43059
Karamyshev, A. L., Patrick, A. E., Karamysheva, Z. N., Griesemer, D. S., Hudson, H., Tjon-Kon-Sang, S., Nilsson, I. M., Otto, H., Liu, Q., Rospert, S. et al. (2014). Inefficient SRP interaction with a nascent chain triggers a mRNA quality control pathway. *Cell* **156**, 146-157. doi:10.1016/j.cell.2013.12.017
Kato, M., Chen, X., Inukai, S., Zhao, H. and Slack, F. J. (2011). Age-associated changes in expression of small, noncoding RNAs, including microRNAs, in C. elegans. *RNA* **17**, 1804-1820. doi:10.1261/rna.2714411
King, R. S. and Newmark, P. A. (2013). In situ hybridization protocol for enhanced detection of gene expression in the planarian Schmidtea mediterranea. *BMC Dev. Biol.* **13**, 8. doi:10.1186/1471-213X-13-8
Kwon, H. C., Bae, Y. and Lee, S.-J. V. (2023). The role of mRNA quality control in the aging of Caenorhabditis elegans. *Mol. Cells* **46**, 664-671. doi:10.14348/molcells.2023.0103
Langmead, B. (2010). Aligning short sequencing reads with Bowtie. *Curr. Protoc. Bioinformatics* Chapter 11, Unit 11 17. doi:10.1002/0471250953.bi1107s32
Langmead, B. and Salzberg, S. L. (2012). Fast gapped-read alignment with Bowtie 2. *Nat. Methods* **9**, 357-359. doi:10.1038/nmeth.1923
Lázaro, E. M., Harrath, A. H., Stocchino, G. A., Pala, M., Baguñà, J. and Riutort, M. (2011). Schmidtea mediterranea phylogeography: an old species surviving on a few Mediterranean islands? *BMC Evol. Biol.* **11**, 274. doi:10.1186/1471-2148-11-274
Li, H., Handsaker, B., Wysoker, A., Fennell, T., Ruan, J., Homer, N., Marth, G., Abecasis, G., Durbin, R., and **Genome Project Data Processing, Subgroup**. (2009). The Sequence Alignment/Map format and SAMtools. *Bioinformatics* **25**, 2078-2079. doi:10.1093/bioinformatics/btp352
Liu, S.-Y., Selck, C., Friedrich, B., Lutz, R., Vila-Farré, M., Dahl, A., Brandl, H., Lakshmanaperumal, N., Henry, I. and Rink, J. C. (2013). Reactivating head regrowth in a regeneration-deficient planarian species. *Nature* **500**, 81-84. doi:10.1038/nature12414
Locascio, S. A., Lapan, S. W. and Reddien, P. W. (2017). Eye absence does not regulate planarian stem cells during eye regeneration. *Dev. Cell* **40**, 381-391.e383. doi:10.1016/j.devcel.2017.02.002
López-Otín, C., Blasco, M. A., Partridge, L., Serrano, M. and Kroemer, G. (2013). The hallmarks of aging. *Cell* **153**, 1194-1217. doi:10.1016/j.cell.2013.05.039
López-Otín, C., Blasco, M. A., Partridge, L., Serrano, M. and Kroemer, G. (2023). Hallmarks of aging: an expanding universe. *Cell* **186**, 243-278. doi:10.1016/j.cell.2022.11.001
Martin, M. (2011). Cutadapt removes adapter sequences from high-throughput sequencing reads. *EMBnet. J.* **17**, 10-12. doi:10.14806/ej.17.1.200
Morita, M. and Best, J. B. (1974). Electron microscopic studies of planarian regeneration. II. Changes in epidermis during regeneration. *J. Exp. Zool.* **187**, 345-373. doi:10.1002/jez.1401870305
Mouton, S., Willems, M., Houthoofd, W., Bert, W. and Braeckman, B. P. (2011). Lack of metabolic ageing in the long-lived flatworm Schmidtea polychroa. *Exp. Gerontol.* **46**, 755-761. doi:10.1016/j.exger.2011.04.003
Nandi, S., Chandramohan, D., Fioriti, L., Melnick, A. M., Hébert, J. M., Mason, C. E., Rajasethupathy, P. and Kandel, E. R. (2016). Roles for small noncoding RNAs in silencing of retrotransposons in the mammalian brain. *Proc. Natl. Acad. Sci. USA* **113**, 12697-12702. doi:10.1073/pnas.1609287113
Newmark, P. A. and Sánchez Alvarado, A. (2000). Bromodeoxyuridine specifically labels the regenerative stem cells of planarians. *Dev. Biol.* **220**, 142-153. doi:10.1006/dbio.2000.9645
Oviedo, N. J., Nicolas, C. L., Adams, D. S. and Levin, M. (2008). Planarians: a versatile and powerful model system for molecular studies of regeneration, adult stem cell regulation, aging, and behavior. *CSH Protoc.* **2008**, pdb.emo101. doi:10.1101/pdb.emo101
Pabis, K., Barardo, D., Sirbu, O., Selvarajoo, K., Gruber, J. and Kennedy, B. K. (2024). A concerted increase in readthrough and intron retention drives transposon expression during aging and senescence. *eLife* **12**, RP87811. doi:10.7554/eLife.87811
Palakodeti, D., Smielewska, M., Lu, Y.-C., Yeo, G. W. and Graveley, B. R. (2008). The PIWI proteins SMEDWI-2 and SMEDWI-3 are required for stem cell function and piRNA expression in planarians. *RNA* **14**, 1174-1186. doi:10.1261/rna.1085008
Pearson, B. J., Eisenhoffer, G. T., Gurley, K. A., Rink, J. C., Miller, D. E. and Sánchez Alvarado, A. (2009). Formaldehyde-based whole-mount in situ hybridization method for planarians. *Dev. Dyn.* **238**, 443-450. doi:10.1002/dvdy.21849
Pedersen, K. J. (1976). Scanning electron microscopical observations on epidermal wound healing in the PlanarianDugesia tigrina. *Wilehm Roux Arch. Dev. Biol.* **179**, 251-273. doi:10.1007/BF00848236
Perrat, P. N., Dasgupta, S., Wang, J., Theurkauf, W., Weng, Z., Rosbash, M. and Waddell, S. (2013). Transposition-driven genomic heterogeneity in the Drosophila brain. *Science* **340**, 91-95. doi:10.1126/science.1231965
Perrigue, P. M., Najbauer, J., Jozwiak, A. A., Barciszewski, J., Aboody, K. S. and Barish, M. E. (2015). Planarians as a model of aging to study the interaction between stem cells and senescent cells in vivo. *Pathobiol. Aging Age Relat. Dis.* **5**, 30052. doi:10.3402/pba.v5.30052

Politz, J. C., Yarovoi, S., Kilroy, S. M., Gowda, K., Zwieb, C. and Pederson, T. (2000). Signal recognition particle components in the nucleolus. *Proc. Natl. Acad. Sci. USA* **97**, 55-60. doi:10.1073/pnas.97.1.55

Rajasethupathy, P., Antonov, I., Sheridan, R., Frey, S., Sander, C., Tuschl, T. and Kandel, E. R. (2012). A role for neuronal piRNAs in the epigenetic control of memory-related synaptic plasticity. *Cell* **149**, 693-707. doi:10.1016/j.cell.2012.02.057

Reddien, P. W. and Sanchez Alvarado, A. (2004). Fundamentals of planarian regeneration. *Annu. Rev. Cell Dev. Biol.* **20**, 725-757. doi:10.1146/annurev.cellbio.20.010403.095114

Reddien, P. W., Oviedo, N. J., Jennings, J. R., Jenkin, J. C. and Sanchez Alvarado, A. (2005). SMEDWI-2 is a PIWI-like protein that regulates planarian stem cells. *Science* **310**, 1327-1330. doi:10.1126/science.1116110

Robb, S. M. C., Gotting, K., Ross, E. and Sanchez Alvarado, A. (2015). SmedGD 2.0: The Schmidtea mediterranea genome database. *Genesis* **53**, 535-546. doi:10.1002/dvg.22872

Ross, K. G., Omuro, K. C., Taylor, M. R., Munday, R. K., Hubert, A., King, R. S. and Zayas, R. M. (2015). Novel monoclonal antibodies to study tissue regeneration in planarians. *BMC Dev. Biol.* **15**, 2. doi:10.1186/s12861-014-0050-9

Rouhana, L., Weiss, J. A., Forsthoefel, D. J., Lee, H., King, R. S., Inoue, T., Shibata, N., Agata, K. and Newmark, P. A. (2013). RNA interference by feeding in vitro-synthesized double-stranded RNA to planarians: methodology and dynamics. *Dev. Dyn.* **242**, 718-730. doi:10.1002/dvdy.23950

Sahu, S., Dattani, A. and Aboobaker, A. A. (2017). Secrets from immortal worms: What can we learn about biological ageing from the planarian model system? *Semin. Cell Dev. Biol.* **70**, 108-121. doi:10.1016/j.semcdb.2017.08.028

Schindelin, J., Arganda-Carreras, I., Frise, E., Kaynig, V., Longair, M., Pietzsch, T., Preibisch, S., Rueden, C., Saalfeld, S., Schmid, B. et al. (2012). Fiji: an open-source platform for biological-image analysis. *Nat. Methods* **9**, 676-682. doi:10.1038/nmeth.2019

Sharma, A. K., Nelson, M. C., Brandt, J. E., Wessman, M., Mahmud, N., Weller, K. P. and Hoffman, R. (2001). Human CD34(+) stem cells express the hiwi gene, a human homologue of the Drosophila gene piwi. *Blood* **97**, 426-434. doi:10.1182/blood.V97.2.426

Shen, D., Coleman, J., Chan, E., Nicholson, T. P., Dai, L., Sheppard, P. W. and Patton, W. F. (2011). Novel cell- and tissue-based assays for detecting misfolded and aggregated protein accumulation within aggresomes and inclusion bodies. *Cell Biochem. Biophys.* **60**, 173-185. doi:10.1007/s12013-010-9138-4

Smith, J., Tyler, S., Thomas, M. B. and Rieger, R. M. (1982). The morphology of turbellarian rhabdites - phylogenetic implications. *T. Am. Microsc. Soc.* **101**, 209-228. doi:10.2307/3225810

Sturm, A., Perczel, A., Ivics, Z. and Vellai, T. (2017). The Piwi-piRNA pathway: road to immortality. *Aging Cell* **16**, 906-911. doi:10.1111/acel.12630

Taylor, R. C. and Dillin, A. (2011). Aging as an event of proteostasis collapse. *Cold Spring Harb. Perspect. Biol.* **3**, a004440. doi:10.1101/cshperspect.a004440

Tu, K. C., Cheng, L.-C., Vu, H. T. K., Lange, J. J., McKinney, S. A., Seidel, C. W. and Sanchez Alvarado, A. (2015). Egr-5 is a post-mitotic regulator of planarian epidermal differentiation. *eLife* **4**, e10501. doi:10.7554/eLife.10501

van Wolfswinkel, J. C. (2014). Piwi and potency: PIWI proteins in animal stem cells and regeneration. *Integr. Comp. Biol.* **54**, 700-713. doi:10.1093/icb/icu084

van Wolfswinkel, J. C., Wagner, D. E. and Reddien, P. W. (2014). Single-cell analysis reveals functionally distinct classes within the planarian stem cell compartment. *Cell Stem Cell* **15**, 326-339. doi:10.1016/j.stem.2014.06.007

Walther, D. M., Kasturi, P., Zheng, M., Pinkert, S., Vecchi, G., Ciryam, P., Morimoto, R. I., Dobson, C. M., Vendruscolo, M., Mann, M. et al. (2015). Widespread proteome remodeling and aggregation in aging C. elegans. *Cell* **161**, 919-932. doi:10.1016/j.cell.2015.03.032

Wang, Y., Zayas, R. M., Guo, T. and Newmark, P. A. (2007). nanos function is essential for development and regeneration of planarian germ cells. *Proc. Natl. Acad. Sci. USA* **104**, 5901-5906. doi:10.1073/pnas.0609708104

Wang, Q., Conlon, E. G., Manley, J. L. and Rio, D. C. (2020). Widespread intron retention impairs protein homeostasis in C9orf72 ALS brains. *Genome Res.* **30**, 1705-1715. doi:10.1101/gr.265298.120

Wenemoser, D. and Reddien, P. W. (2010). Planarian regeneration involves distinct stem cell responses to wounds and tissue absence. *Dev. Biol.* **344**, 979-991. doi:10.1016/j.ydbio.2010.06.017

Wenemoser, D., Lapan, S. W., Wilkinson, A. W., Bell, G. W. and Reddien, P. W. (2012). A molecular wound response program associated with regeneration initiation in planarians. *Genes Dev.* **26**, 988-1002. doi:10.1101/gad.187377.112

Wood, J. G. and Helfand, S. L. (2013). Chromatin structure and transposable elements in organismal aging. *Front. Genet.* **4**, 274. doi:10.3389/fgene.2013.00274

Wrona, F. J. (1986). Distribution, abundance, and size of rhabdoids in dugesia-polychroa (Turbellaria, Tricladida). *Hydrobiologia* **132**, 287-293. doi:10.1007/BF00046262

Wu, Q., Ma, Q., Shehadeh, L. A., Wilson, A., Xia, L., Yu, H. and Webster, K. A. (2010). Expression of the Argonaute protein PiwiL2 and piRNAs in adult mouse mesenchymal stem cells. *Biochem. Biophys. Res. Commun.* **396**, 915-920. doi:10.1016/j.bbrc.2010.05.022

Wurtzel, O., Cote, L. E., Poirier, A., Satija, R., Regev, A. and Reddien, P. W. (2015). A generic and cell-type-specific wound response precedes regeneration in planarians. *Dev. Cell* **35**, 632-645. doi:10.1016/j.devcel.2015.11.004

Wurtzel, O., Oderberg, I. M. and Reddien, P. W. (2017). Planarian epidermal stem cells respond to positional cues to promote cell-type diversity. *Dev. Cell* **40**, 491-504.e495. doi:10.1016/j.devcel.2017.02.008

Yang, J.-H., Hayano, M., Griffin, P. T., Amorim, J. A., Bonkowski, M. S., Apostolides, J. K., Salfati, E. L., Blanchette, M., Munding, E. M., Bhakta, M. et al. (2023). Loss of epigenetic information as a cause of mammalian aging. *Cell* **186**, 305-326.e327. doi:10.1016/j.cell.2022.12.027

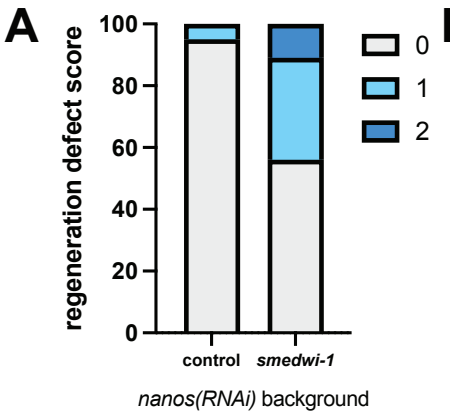

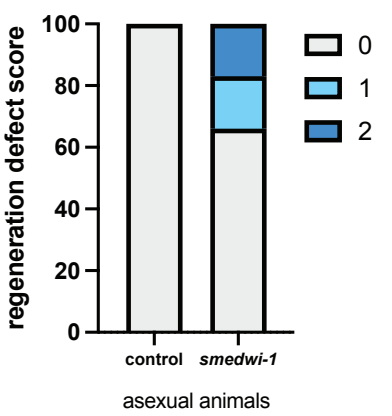

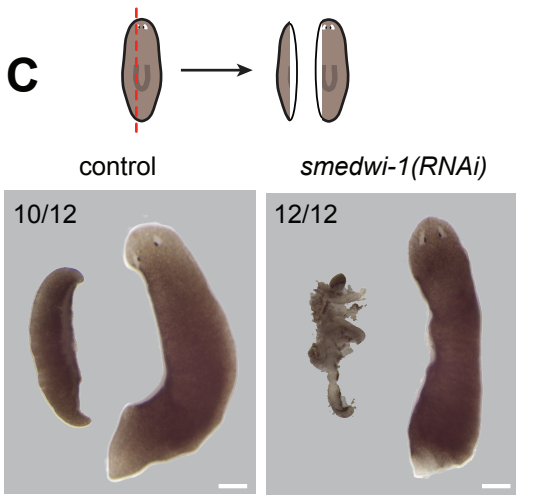

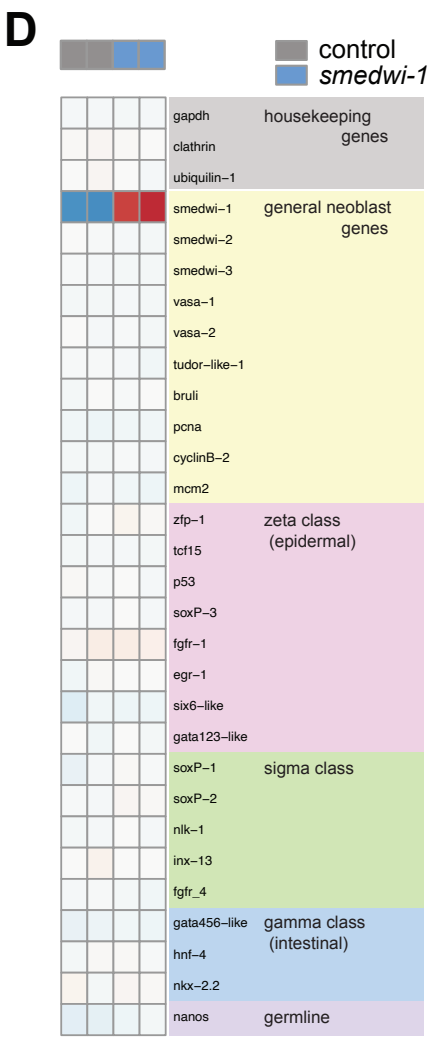

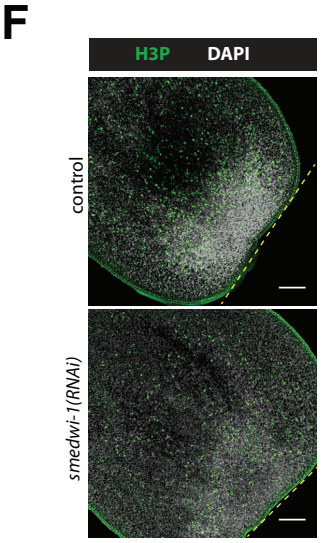

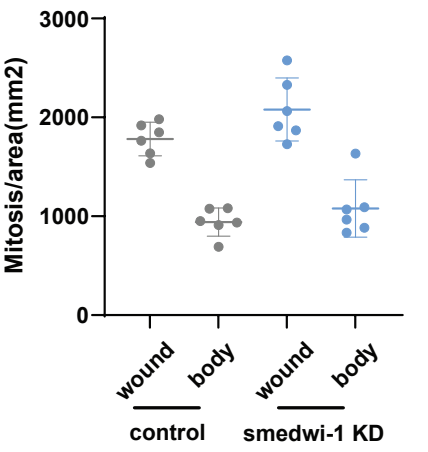

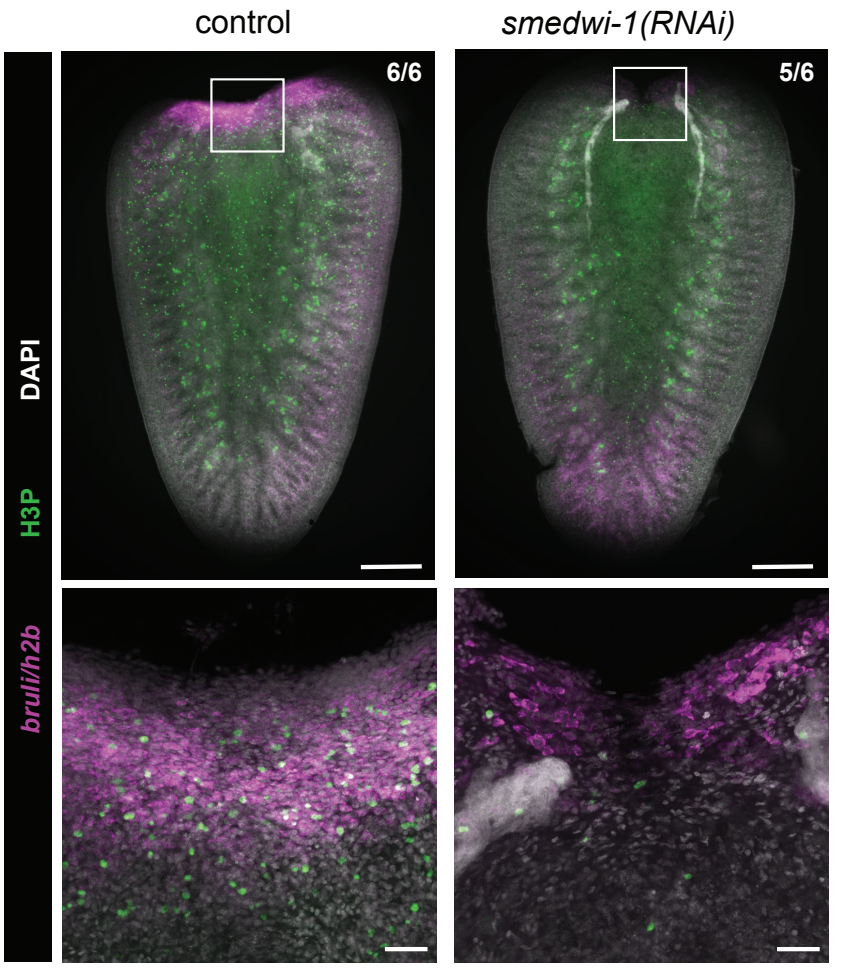

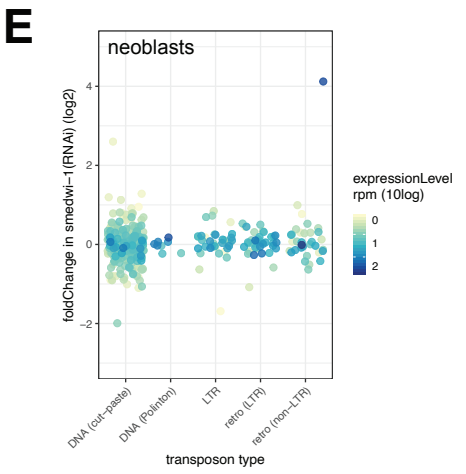

Fig. S1. (Ad Fig. 1)

A. Quantification of the frequency of observed wound healing phenotypes at d3 post amputation of sexual animals treated for 3 months with *nanos(RNAi)* to eliminate the germline, or with *nanos-smedwi-1(doubleRNAi)* treatment. Wound size was around 3mm. >20 animals per condition. Fisher's exact test, * $p<0.05$, **** $p<0.0001$.

B. Quantification of the frequency of observed wound healing phenotypes at d3 post amputation of asexual animals after 2 months of the *smedwi-1(RNAi)* treatment. Wound size was around 2mm. >20 animals per condition. Fisher's exact test, * $p<0.05$, **** $p<0.0001$.

C. Image of asexual control or *smedwi-1(RNAi)* animal at 24 hours after parasagittal section. Among control animals 10 out of 12 small lateral fragments survived and eventually regenerated. Among the *smedwi-1(RNAi)* animals all small lateral fragments lysed within 24 hours.

D. Heatmap of RNA expression levels of control genes and neoblast genes in control and *smedwi-1(RNAi)* neoblasts as determined by RNAseq analysis. Shown are log2 fold changes relative to the averaged expression.

E. Effect of long-term loss of SMEDWI-1 on transposon levels in isolated neoblasts. Transposons are classified by type and their baseline expression level is shown by coloring. No major changes in transposon levels are detected.

F. Immunofluorescence of phosphorylated histone 3 (H3P) in small tail pieces at day 3 after amputation (right), and quantification of the density of mitotic figures (left) in *smedwi-1(RNAi)* animals compared to controls. Scale bar, 300µm. Datapoints represent biological replicates (n=6).

G. (expanded from main Fig. 1f) Immunofluorescence of phosphorylated histone 3 (H3P) and FISH of *bruli* and *h2b* to mark neoblasts at day 3 after amputation of large posterior fragments. *smedwi-1(RNAi)* fragments have reduced accumulation of neoblasts at the wound site. Some background staining (out of focus) is present in the tail region of the animals. Clusters of H3P cells located along the flanks of the animals reflect the testes. White tracks at the top of the *smedwi-1(RNAi)* fragment are the sperm ducts. Scale bar, 1mm (top panels), or 50µm (bottom panels).

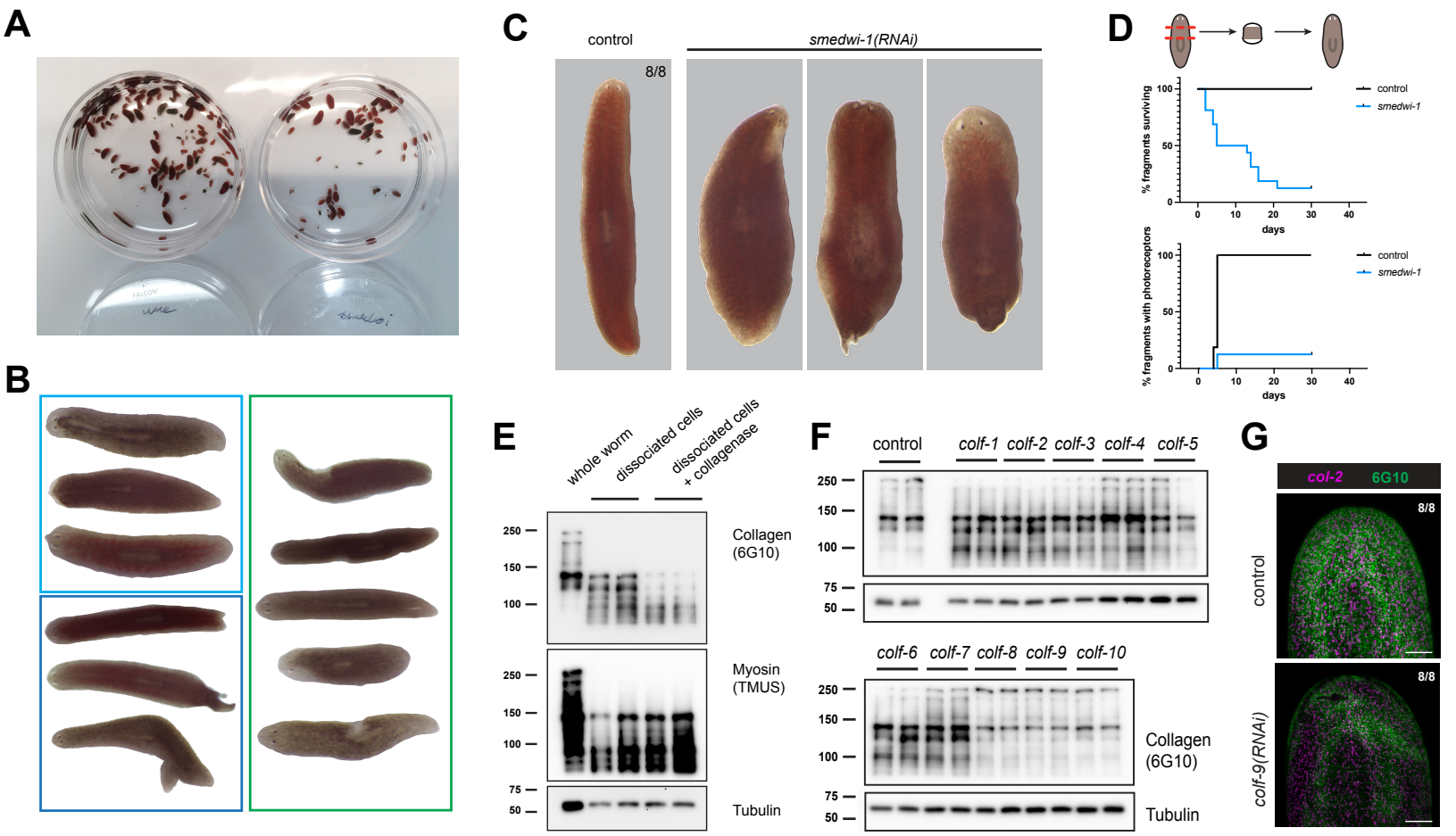

Fig. S2. (Ad Fig. 1)

In this study we focused on the wound regeneration phenotype that develops over time in *smedwi-1(RNAi)* animals. We did however observe several other signs of decreased health and increased fragility in these animals over time. We did not detect overt lethality among uninjured homeostatic *smedwi-1(RNAi)* animals when cultured in the presence of the antibiotic Gentamycin. However, in the *smedwi-1(RNAi)* asexual cultures the various non-regenerating fragments that were formed over the course of the animal culture eventually died, and fragments with large wound surfaces frequently lysed and dissolved (see for example **Fig. S1C**). In agreement with this, even in the absence of intentional amputations, colonies on *smedwi-1* dsRNA expanded notably less than colonies on control dsRNA.

Further, we found that homeostatic *smedwi-1(RNAi)* animals became more sickly than control RNAi animals over time, and showed increased incidence of morphological aberrations (found in around 15% of long-term *smedwi-1(RNAi)* animals whereas they are very rare (<1%) in controls. Further, in the absence of antibiotics, lysis of cut fragments and development of abnormalities was exaggerated in the *smedwi-1(RNAi)* animals, whereas no changes were observed in the controls, indicating that the *smedwi-1(RNAi)* animals were more fragile in the face of microbial challenges.

A. Illustration of the reduced expansion of *smedwi-1(RNAi)* asexual cultures compared to controls. Each culture was started as a cohort of 20 asexual worms and maintained on weekly feedings with control food or *smedwi-1* dsRNA for 6 months. The culture on control food expanded significantly more than the culture on *smedwi-1*dsRNA.

B. Illustration of the morphological aberrations developed in *smedwi-1(RNAi)* asexual cultures over time. Animals had been maintained on weekly feedings with *smedwi-1* dsRNA for 6 months. Animals with aberrations in head morphology (light blue box), tail morphology (dark blue box), or pigmentation defects (green box) were readily detected in the population whereas no such animals were found among controls.

C. Groups of eight 2-month control or *smedwi-1(RNAi)* asexual animals were maintained in planarian water without the antibiotic Gentamycin for 4 weeks. The control animals showed no defects, but out of the 8 *smedwi-1(RNAi)* animals, 2 shrunk and died, and 3 (shown) developed morphological defects.

D. Progression of regeneration of small tissue fragments (double wound site) from asexual animals in the absence of the antibiotic Gentamycin. Control tissue fragments all survived and regenerated heads with detectable eye spots in 5 days. Of the *smedwi-1(RNAi)* tissue fragments only 2 out of 16 regenerated a head and survived. The remaining *smedwi-1(RNAi)* fragments either lysed or aborted regeneration and shriveled away.

E. Treatment of macerated planarian cells with collagenase resulted in a reduction of the 6G10 signal on Western blot, suggesting that 6G10 recognizes an extracellular protein. Intracellular proteins Tubulin and Myosin were not affected by collagenase treatment.

F. Western blot of asexual animals treated with dsRNA against fibrillar collagens 1-10, labeled by the 6G10 antibody. Biological duplicates are shown. Knockdown of *colf-8*, *colf-9* and *colf-10* resulted in reduced signal on the blot.

G. Immunofluorescence of animals treated with dsRNA against *colf-9* showed no change in the number of muscle cells as marked by *collagen-2* mRNA, but showed reduced staining by antibody 6G10. Scale bar, 100μm.

While the exact epitope for the 6G10 antibody remains unknown, based on our data we propose that the target is a collagen.

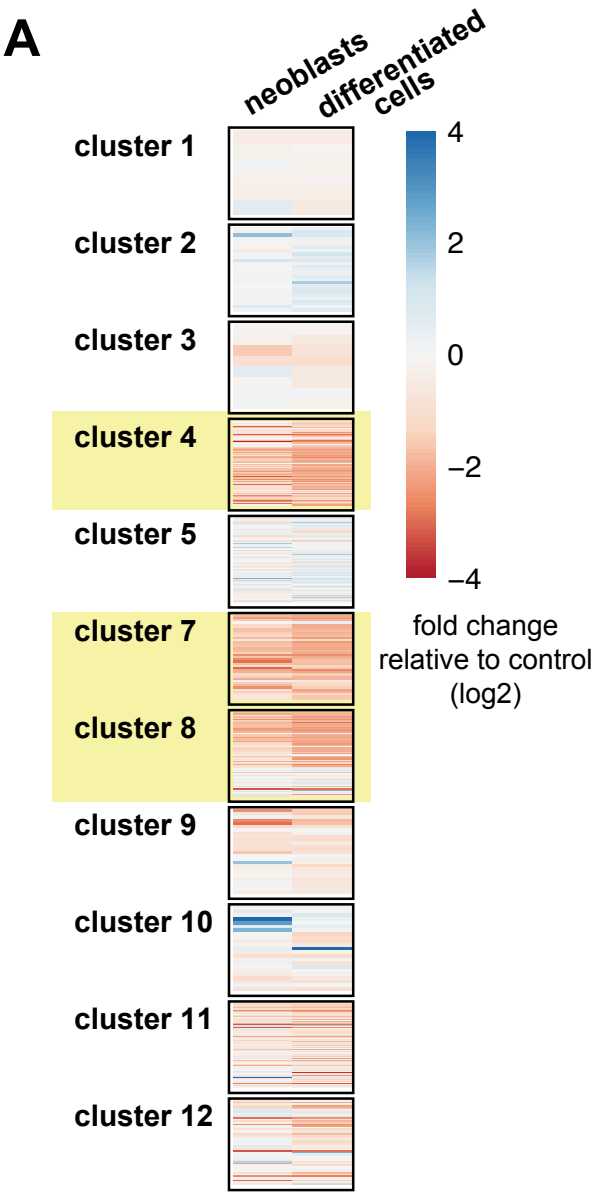

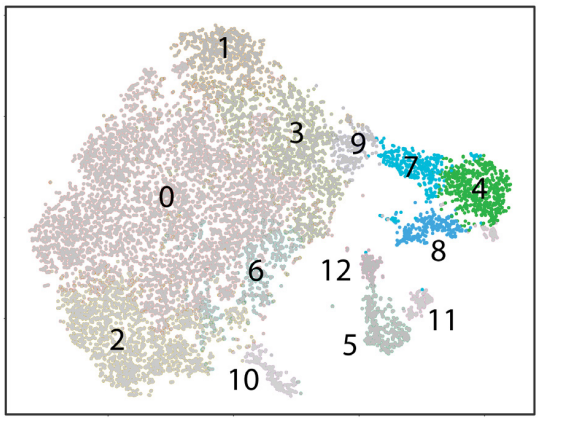

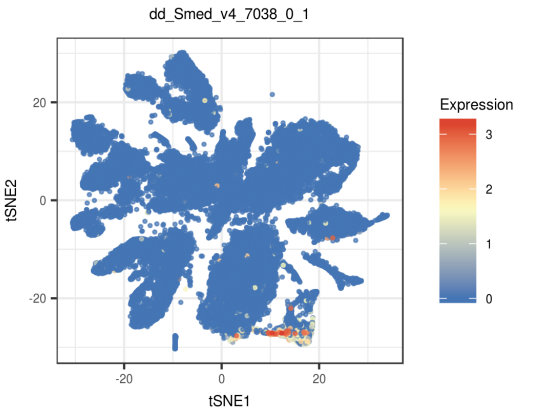

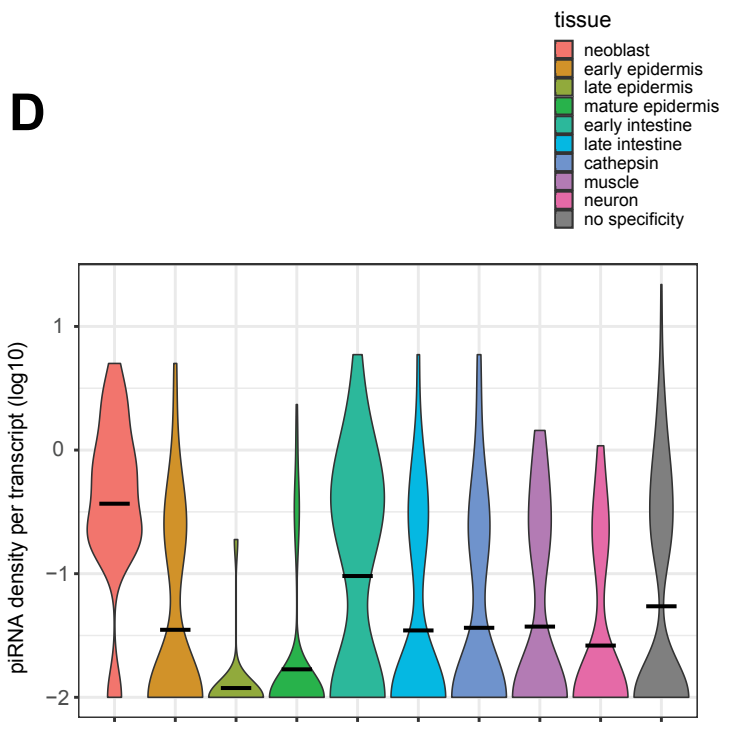

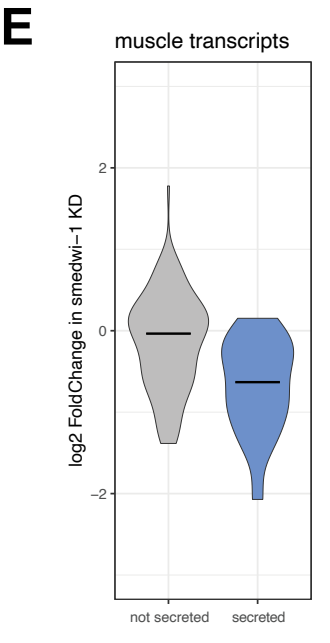

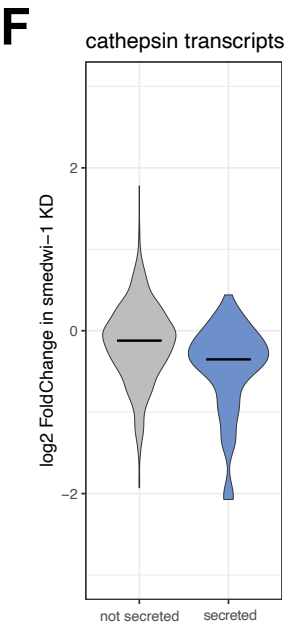

Fig. S3. (Ad Fig. 3)

A. (expanded version of main Fig. 3b) Analysis of genes characteristic for subclusters of epidermal cells as determined by single cell sequencing (Fincher et al., 2018), shows that transcripts altered in *smedwi-1(RNAi)* animals are largely confined to a few clusters, which mark a late epidermal precursor stage, known as "category 3 cells".

B. UMAP representation of the epidermal subclusters (Fincher *et al.*, 2018) showing that affected transcripts are found in a specific subset of epidermal cells.

C. UMAP representation of total cells (top, (Fincher *et al.*, 2018)) and epidermal subclusters (bottom, (Fincher *et al.*, 2018)) marking the cells that show expression of the transcription factor EGR-5. EGR-5 expression is restricted to a specific group of cells, known as the "category 3 cells".

D. Violin plot showing the density of piRNAs per transcript in each cell type of wildtype animals. Horizontal bars indicate the median number of piRNAs per transcript for each tissue. Transcripts that are specific to late epidermal precursors tend to have low levels of matching piRNAs.

E. Violin plot showing the distribution of fold changes in *smedwi-1(RNAi)* animals relative to controls, of muscle cell transcripts encoding secreted and non-secreted proteins.

F. Violin plot showing the distribution of fold changes in *smedwi-1(RNAi)* animals relative to controls, of cathepsin cell transcripts encoding secreted and non-secreted proteins.

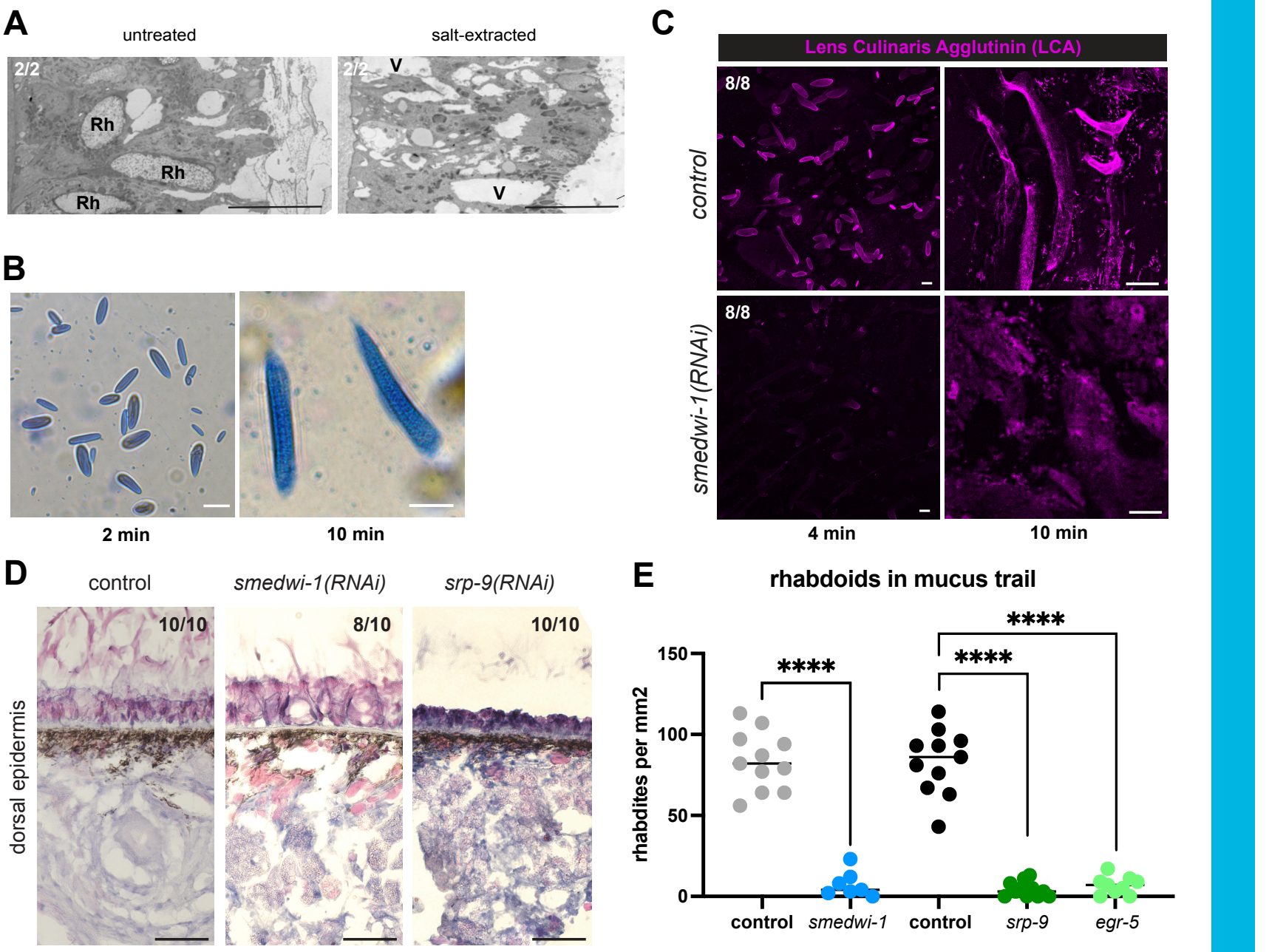

Fig. S4. (Ad Fig. 4)

Rhabdoids, or rhabdites-like structures, are rod-shaped epidermal secretory inclusions that characterize the Rhabditophora to which planarians belong, and exist in at least two types. Epidermal rhabdoids are large structures produced by cells in the epidermal layer, and upon secretion swell to produce the mucus that covers the epidermis (Hayes, 2017; Wrona, 1986). Adenal rhabdites are smaller in size and are produced from gland cells located in the subepidermal space (Smith et al., 1982). Both types of structures may be secreted upon stress and injury and may assist in physical barrier formation and microbial defense. Additional epidermal inclusions such as Hyman vesicles (Cheng et al., 2018) have been described.mi Rhabdites/rhabdoids have been primarily described based on EM imaging. Connecting the structures observed in the fixed tissues of EM images to the structures secreted from live planarians is problematic, especially as the secreted structures rapidly change shape. In EM images, the rhabdites are visible as large granules of 2-10µm in length with fibrillar or speckled content. Additionally, smaller (1-2µm) rod-shaped structures with more dense, often laminar content are present in the epidermal cells. It is possible that these smaller structures are precursors to the larger rhabdites, but it is also possible that their biogenesis is independent. Another possibility is that the large rhabdites actually represent partially swollen versions of the smaller structures.

Rhabdites from live animals can be observed in mucus trails or epidermal scrapes. Additionally, rhabdites are efficiently secreted upon exposure of the animals to high salt media. Immediately after secretion (in mucus trails or upon salt extraction), rod-like structures of around 10µm in length are detected, as well as some smaller rod-shaped structures. Within a few minutes, the structures swell up and rapidly turn into smears of mucus that merge with each other or form fibrous connections over long distances.

A. Electron microscopy image of salt-extracted epidermal cells shows the absence of larger rhabdoid structures (Rh) that were found in control epidermal cells, and instead shows empty spaces (V) in the epidermal tissue. This suggests that the larger rod-shaped inclusions are the primary structures that are secreted. We however cannot determine whether the smaller rod-shaped structures observed in the epidermis also contribute to the secreted objects. To avoid misnaming the structures, we therefore chose to refer to all rod-shaped secreted objects as "rhabdoids", intending this to mean rhabdite-like structures. This naming is in accordance with previous literature (e.g. (Smith *et al.*, 1982)).
The rhabdoids that were lost from the epidermis after salt extractions were between 2 and 8µm in length. Scale bar, 10µm. **B.** Aniline blue staining of the structures secreted after salt extraction. Rhabdoids of ~10µm in length were detected immediately after secretion, and rapidly increased in size. Scale bar, 10µm. **C.** Labeling of the structures secreted after salt extraction with the Rhodamine-coupled lectin LCA. Labeling shows rhabdoids of ~10µm in length immediately after secretion, that rapidly increased in size and spread out across the surface. The structure of rhabdoids from *smedwi-1(RNAi)* animals was altered and contained fewer glycoproteins that were labeled by LCA. Scale bar, 10µm.
D. (expanded from main Fig. 4a, to include the *srp-9(RNAi)* sample) Transverse sections stained with Hematoxylin and Eosin (H&E) show the altered structure of the epidermis in *smedwi-1(RNAi)* animals, including a less pronounced basement membrane (BM), and subepidermal accumulations of material (black arrowheads). Scale bar, 50µm.
E. (ad main Fig. 4d) Quantification of the secreted rhabdoids indicates a reduction of rhabdoids in *smedwi-1(RNAi)* animals, *egr-5(RNAi)* animals, and *srp-9(RNAi)* animals. Separate sets of controls were used. Datapoints represent biological replicates (n=10-12). Statistics are based on t-test. **** $p<0.0001$.

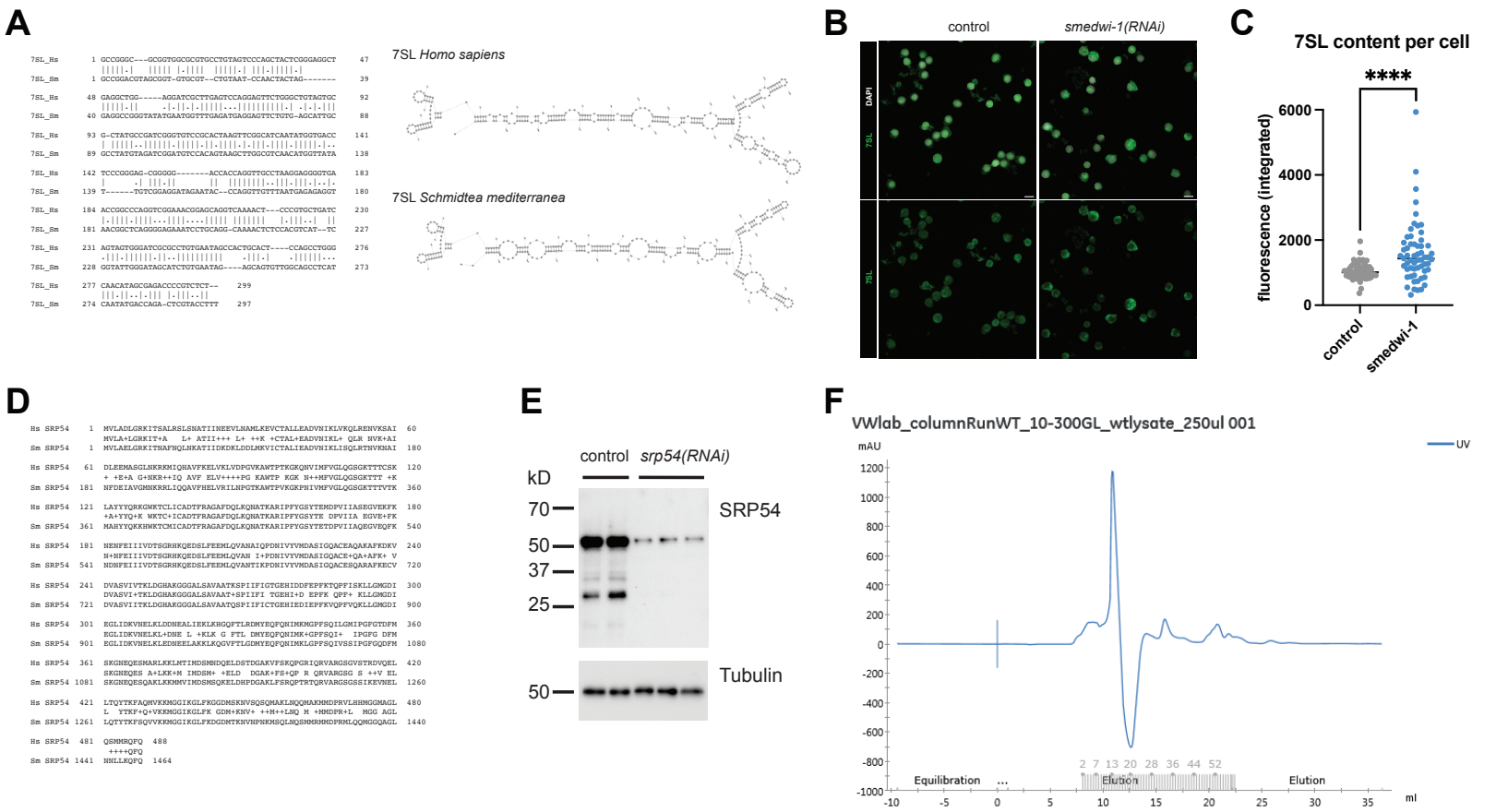

Fig. S5. (Ad Fig. 5)

A. Alignment (left) and predicted structure (right, RNAfold) of the human 7SL RNA and the predicted 7SL RNA from *Schmidtea*. The sequence diverges (62% identity), but the structure is highly conserved.

B. (expanded view from Fig. 5c) RNA FISH for the *7SL* RNA on isolated cells shows increased intensity and prominent accumulation of the RNA in the cytoplasmic space in *smedwi-1(RNAi)* samples compared to controls. Scale bar, 10µm.

C. Quantification of the 7SL signal per cell. Statistics are based on t-test. **** $p<0.0001$.

D. Alignment of protein sequence of *S. mediterranea* SRP54 to human SRP54 protein.

E. Western blot of control and *srp54(RNAi)* samples labeled with the SRP54 antibody shows a major band around 54kD in planarian lysate, that is strongly reduced upon *srp-54* knockdown, confirming antibody specificity.

F. UV trace of gel filtration column showing the full spectrum of the elution and the fractionation strategy.

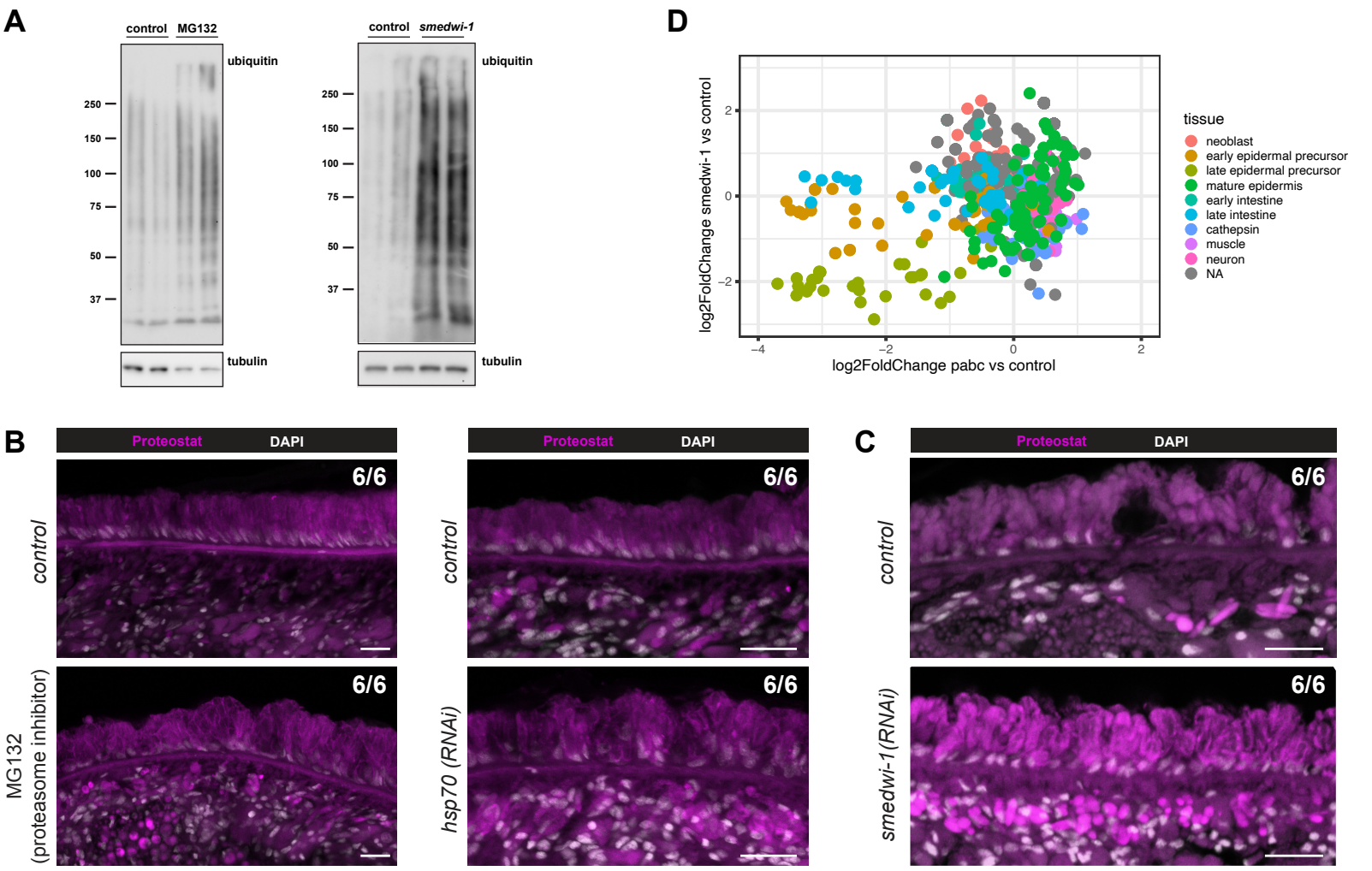

Fig. S6. (Ad Fig. 6, Discussion)

A. Western blot labeled with antibody against ubiquitin shows proteins targeted for degradation. Chemical inhibition of the proteasome by MG132 resulted in a mild increase in ubiquitinated protein, verifying the detection method. Long-term absence of SMEDWI-1 resulted in a stronger increase in ubiquitinated protein. Shown are biological replicates.

B. Transverse sections stained with the aggregation-specific protein dye Proteostat show an increase in labeling upon exposure of animals to the proteasome inhibitor MG132 or upon knockdown of the protein chaperone *hsp-70*.

C. Transverse sections stained with Proteostat show the increased presence of protein accumulations in *smedwi-1(RNAi)* animals in the epidermal cells and in the subepidermal space (arrowheads). Scale bar, 20µm.

D. Comparison of log2 FoldChanges of tissue-specific transcripts between *smedwi-1(RNAi)* samples and *pabp(RNAi)* samples (Bansal et al., 2017).

Table S1.

qPCR primers

	FW	RV
smedwi-1	GTCTCAGAAAACAACTAAAGGTACAGCA	TGCTGCAATACACTCGGAGACA
nanos	GGCCATGCTTCCAACAATGC	TTGCAAAGACAGATTTTTCACTGTTAGA
egr2	ACCGGTCGTCAGATGGATCC	CGCGATCTCATGAGCACAACA
egr3	ACCCCTTCTCCAATGGATTGC	TGAGACGAATCTGGAATAATTGTGGA
runt1	GTCGGCGAGTAATCCGTCGA	TATTTTCCTCTTCCACTGCGACTGA
h2b	GCATCTGAGGCAAGCAAATTGGGAGAAAGTTG/	TCAACGACGTTTTAAAAGTTCAGAACA
wntP1	GCTCAAACTGTCGCTGAGGC	CGTTGTCGTCACATCCTTGCC
wntless	TCGTCAGTCAGATTGATGAAAGTCA	TGACGTAGAAATTCCACATGCCA
prog-1	GCAATCTGCTTTCGTAATGTGTCCT	TCTGCAAAGTCTCCCGCCAA
c11136	TGCTCTTCGCAGCAATTGTGA	TGCCGAACCGCATTTGCTTT
c11136-pre	ACCGCATCCATGGATCACGT	TGCCGAACCGCATTTACTGAAAAA
c7016	TCGGCTTGTTAATTCTCAACGGC	CGGCTTCTTCTGTTACTTCAAAATTTCC
c7016-pre	CAAAGGAAATTTTGGTGTGATTTATTGAGT	CCATTTCTTATCTCCTTGAATTTCGGC
c2926	TGTGGAAACCAAGGACAATTCAGAAT	ACAAGAACCATAACAAAGTCGGAAGT
c2926-pre	CAAGGATGTGGAAACCAAGGACA	AAATCAAACATTTAACACTTTAAAGTCGCA
c6175	TGTTCTCCACGATGTGACTTGGA	TTGCCGCATATCCACCGTTG
c9505	AATGTTGAATCACGACAAACGGCT	AAGCTGACACGCACCAGTTG
vimentin	AACCGCGGCTTCAACTGAAC	CAGCGGAACTTAAAACTCGCTCTT
PRSS12	TCGAGATATTATTGGGATTCCGCA	CGGTTACGGTTGAGTATTGAGGA
c9830	TGCACTTGGTGAGGTTTTCGG	CCTTGTCCATTTTCCTCCTGGG
d558	TGGTGCTCCAATGATGAGGGA	TCTTTTGTTCTTTTTCACTTTCAGCGA
c5568	TGTTTTAATCGGTTTAGTGGCAATCGT	CCTTCAAGTCTTCGAACTCATTCAAAAG
b-gal	CTTGCGGTTCTTCTGATAGACGT	TCAGTCCACGGACCACATCA
hspA8	GAAATCGCACAACGCCCAGT	CAATCGCTTTGCATCAAAAACCGT
atg1	TCACGGTCGACCCTCCTAGA	GGCGTCAGATTTTGGTTGTGGT

cloning primers

	FW	RV
egr-5	CTGTTTCTCCCTTGATACTCCCA	ACGTATTCGGGATTTTGAACGG
srp-9	TTAGCCGATCCTTCTAAATGCAG	AATGCAAAATTATGCTCTTGAGGC
srp-54	AGCTGTTGGAATGAATAAACGTCG	TAGAGATTGTCGCGATGGCC
c6175	TGTCAAAACTTTCGATCTTTGCGT	GGAGCTTTCAGTCTCCTTGAAC
c9505	GCAAACGTCAAAGAAATGCGAC	GCCTTTGTTCCTTCCAGTGC
colf-1	TTGGTGGCTCAGGACCTCT	TTCTGACCGGACGTTCACTG
colf-2	TCTAACCGGTCCAAATGGCT	ATGGACCAAGATCTCCCGGA
colf-3	CCCGGCTTTCCTGGTAAGAA	CACCGACAACCTACTGCAGT
colf-4	TGACTATGGGAAGATCAGGTGA	TGAGGTCCAGGATCTCCAGG
colf-5	TCTTCAGGCTCACCAGGTCT	TCTTTACCGGCTGGACCAAC
colf-6	TGGAAATCCCGGTGAAGATGG	TTCCTTGTGGGCCAGGTTTT
colf-7	TGGGATTTCCTGGCATTGCA	CCTCTAGACCAGGGCTTCCT
colf-8	AGGTGATCCTGGACCTAAAGGA	CCATCAAGCCCATTGGACCT
colf-9	TGACAGCTGTACAAATTTCGGA	AATGCCTCTTGGACCCGAAG
colf-10	AGATGCATCCCATTCAATGTCT	CCCGGGTTTCCTCCAATACC
hsp70	CGCTGAACGCAATGTGTTAA	CTTGTTTTCCAGCCCCTCCT

probes

	RC
7SL	CTCTCATTAAACAACCTGGGTATTCTATCCTCCGACAATATAACCATGTTGAC
tRNA	ATGAGACTAAATCAAACATTATCTCCAAGTTAACAGCTTGGAATTTTTAATAAACTAAGTCTC

References

Bansal, D., Kulkarni, J., Nadahalli, K., Lakshmanan, V., Krishna, S., Sasidharan, V., Geo, J., Dilipkumar, S., Pasricha, R., Gulyani, A., et al. (2017). Cytoplasmic poly (A)-binding protein critically regulates epidermal maintenance and turnover in the planarian Schmidtea mediterranea. Development *144*, 3066-3079. 10.1242/dev.152942.

Cheng, L.C., Tu, K.C., Seidel, C.W., Robb, S.M.C., Guo, F., and Sanchez Alvarado, A. (2018). Cellular, ultrastructural and molecular analyses of epidermal cell development in the planarian Schmidtea mediterranea. Dev Biol *433*, 357-373. 10.1016/j.ydbio.2017.08.030.

Fincher, C.T., Wurtzel, O., de Hoog, T., Kravarik, K.M., and Reddien, P.W. (2018). Cell type transcriptome atlas for the planarian Schmidtea mediterranea. Science *360*. 10.1126/science.aaq1736.

Hayes, M.J. (2017). Sulphated glycosaminoglycans support an assortment of planarian rhabdite structures. Biol Open *6*, 571-581. 10.1242/bio.024554.

Smith, J., Tyler, S., Thomas, M.B., and Rieger, R.M. (1982). The Morphology of Turbellarian Rhabdites - Phylogenetic Implications. T Am Microsc Soc *101*, 209-228.

Wrona, F.J. (1986). Distribution, Abundance, and Size of Rhabdoids in Dugesia-Polychroa (Turbellaria, Tricladida). Hydrobiologia *132*, 287-293. Doi 10.1007/Bf00046262.